Sulfatase modifying factors control the timing of zebrafish convergence and extension morphogenesis

Ailen Soledad Cervino[1,2], Amrita Basu[3], Ryan J. Weiss[3,4], Gursimran Kaur Bajwa[5,6], Rubén Marín Juez[5,6], Sandra Grimm[1,2], Cristian Coarfa[1,2], and Margot Kossmann Williams[1,2]*

[1] Center for Precision Environmental Health, Baylor College of Medicine, Houston, TX, USA

[2] Department of Molecular & Cellular Biology, Baylor College of Medicine, Houston, TX, USA

[3] Complex Carbohydrate Research Center, University of Georgia, Athens, GA, USA

[4] Department of Biochemistry and Molecular Biology, University of Georgia, Athens, GA, USA

[5] Centre de Recherche Azrieli, Centre Hospitalier Universitaire Sainte-Justine, Montréal, QC, Canada

[6] Department of Pathology and Cell Biology, Faculty of Medicine, Université de Montréal, QC, Canada

* Author for correspondence: margot.williams@bcm.edu

ABSTRACT

To shape the emerging body plan, morphogenetic cell movements must be coordinated not only in space, but also in time. Convergence and Extension (C&E) movements that elongate the anteroposterior axis initiate with precise timing during vertebrate gastrulation, but the mechanisms controlling their onset remain unknown. We examined this question using zebrafish embryonic explants that faithfully recapitulate C&E cell movements and their precise timing in culture, in isolation from other gastrulation movements. We determined that new transcription is required at gastrulation onset for C&E in explants and identified *sulfatase modifying factor 2* (*sumf2*) as a candidate 'trigger' gene expressed at this time. *sumf2* and its paralog *sumf1* encode negative and positive regulators, respectively, of all sulfatase enzymes, which remove sulfate groups from their substrates, altering their biological activity. In zebrafish embryos and explants, *sumf1 and sumf2* expression levels invert at gastrulation onset, predicting a reduction in sulfatase activity and consequent increase of substrate sulfation. We found that overexpressing *sumf1* and *sumf2* causes delayed or precocious C&E onset, respectively, whereas loss of *sumf1* and *sumf2* function shifts C&E timing in the opposite direction. We further identified Sulf1, an extracellular sulfatase that modifies heparan sulfate proteoglycans (HSPGs), as the key effector by which *sumf1* and *sumf2* control C&E timing. Accordingly, reduced or increased levels of sulfated heparan

sulfate similarly shift C&E onset and suppress *sumf1* and *sumf2* mutant phenotypes. Together, our work supports a model in which *sumf2* expression at zebrafish gastrulation onset reduces sulfatase activity, rewriting HSPG sulfation patterns to promote and/or permit C&E morphogenesis.

Key words: convergence and extension, gastrulation, HSPGs, Sumf1, Sumf2, Sulf1, zebrafish

INTRODUCTION

Morphogenetic cell movements must be coordinated not only in space, but also in time to properly shape the embryonic body plan. Indeed, changes in the timing of developmental events, termed heterochrony, can underlie malformations in individuals and fuel evolutionary change in populations (*1, 2*). One striking example of morphogenetic timing is the onset of gastrulation cell movements that form the primordial germ layers and shape them into the nascent embryonic axes. In many species, multiple gastrulation movements occur simultaneously and/or in rapid succession, such that the absolute timing of one process is necessary to preserve its timing relative to the others. For example, many teleost fish and amphibian embryos exhibit epiboly (which thins and spreads the epiblast), internalization (which brings mesoderm and endoderm germ layers inside the embryo), and convergence & extension (C&E) (which elongate the anteroposterior axis) movements simultaneously. The onset of epiboly in zebrafish is thought to result from a rapid fluidization of the epiblast, a consequence of cell rounding during meta-synchronous cell cleavages (*3, 4*). Initial internalization of mesoderm and endoderm cells may be triggered by a threshold level of Nodal signaling activity (*5*), which promotes cell protrusions that “un-jam” cells to enable them to ingress at the margin (*6*) or ectopically (*7*). Once leader cells ingress at the margin, “followers” in adjacent spatial domains subsequently internalize in a temporally ordered fashion according to their expression of *hox* genes (*8*), similar to a mechanism reported during chick gastrulation (*9*). However, mechanisms controlling the timing of C&E morphogenesis remain elusive.

C&E movements simultaneously narrow and elongate embryonic tissues via polarized cell rearrangements, providing the major driving force of anteroposterior (AP) axis extension and, in many species, neural tube closure (*10-13*). C&E are driven by polarized cell behaviors including mediolateral (ML) cell elongation and

57 alignment, ML-biased cell protrusions, and polarized contraction of cell interfaces by which cells exchange
58 neighbors to form a longer and narrower array (*14, 15*). Vertebrate C&E movements and/or their underlying ML
59 intercalation behaviors often begin at mid-gastrulation (*16-18*). In zebrafish, this is marked by a switch in the
60 trajectory of cell movements toward the embryo's dorsal side at ~75% epiboly (~8 hours post fertilization (hpf))
61 (*18, 19*). Evidence suggests that these movements do not result from chemotaxis (*20*), but rather from spatially
62 restricted cell-cell interactions whose domains are defined by morphogen signaling gradients (*21-23*). The
63 signature ML polarity of vertebrate C&E behaviors is under control of planar cell polarity (PCP) signaling, which
64 orients cell behaviors with respect to the embryonic axes (*24, 25*). This results from the polarized membrane
65 localization of core PCP signaling components (*26-29*), which directly precedes the onset of C&E cell
66 behaviors (*22, 30*). The precision and coordination of these events imply the existence of a timing cue that
67 determines the onset of C&E cell behaviors. Several morphogen signaling pathways are essential for C&E,
68 with BMP preventing C&E of the ventral mesoderm (*21, 31, 32*) and Nodal and FGF signaling promoting C&E
69 dorsally (*22, 33-37*). However, all these pathways are active hours before C&E begins at mid-gastrulation,
70 suggesting that their activity might not be directly responsible for the timing of C&E onset. Indeed, although
71 Activin (which signals through the Nodal pathway) was sufficient to induce axial mesoderm exhibiting C&E in
72 *Xenopus* animal cap explants, the timing of C&E remained constant regardless of when Activin was applied
73 (*38*). This suggests that the timing mechanism functions in parallel with known C&E regulators, but its
74 molecular basis is unknown.
75 Mechanisms controlling the timing of other early embryonic events have been extensively studied,
76 including early cell cycles and zygotic genome activation (ZGA). For example, early cell cleavages are
77 controlled by cyclical expression and degradation of maternally expressed Cyclins (*39*). After a set number of
78 cell divisions, ZGA is triggered by a threshold nuclear/cytoplasmic (N/C) ratio (*40, 41*) (*41-43*), which is thought
79 to function through titration of histones and other nuclear factors (*42-45*). In amphibian embryos, the timing of
80 gastrulation was linked not to fertilization or ZGA, but to the first embryonic cleavage (*46, 47*), and this timing is
81 reportedly regulated predominantly by cytoplasmic factors (*46, 48-50*). However, the onset of gastrulation
82 morphogenesis is unchanged in embryos with varying cell size and cell cycle length (*50-53*), making
83 mechanisms that count cell cycles or measure N/C ratios unlikely regulators of C&E timing. Zebrafish

84 gastrulation morphogenesis requires zygotic transcription (*54*), but its timing is uncoupled from that of ZGA,
85 instead supporting a model by which new gene expression triggers C&E at a specific time.
86 Using a reductive zebrafish embryonic explant model in which C&E is isolated from the other gastrulation
87 cell movements, we determined that new transcription is required at gastrulation onset for C&E to occur, and
88 that *sulfatase modifying factor 2* (*sumf2*) is initially expressed during this critical window in both explants and
89 intact embryos. *sumf1* and *sumf2* encode Formylglycine Generating Enzyme (FGE) (*55-58*) and its antagonist
90 and paralog pFGE (*59-61*), respectively, a pair whose balance determines the activity of every sulfatase
91 enzyme in the body (*62-65*). *sumf1* is maternally expressed, and its transcript abundance drops just as *sumf2*
92 is expressed at gastrulation onset, inverting *sumf1/sumf2* levels and altering sulfation in the embryo. We show
93 that overexpression of *sumf1* and *sumf2* causes delayed or precocious C&E onset, respectively, in both
94 explants and embryos, whereas loss of *sumf1* and *sumf2* function shifts C&E timing in the opposite direction.
95 We further identified Sulf1 as a key sulfatase by which Sumf1 and Sumf2 modify C&E timing. Reduced or
96 increased levels of sulfated heparan sulfate, the predominant substrate of Sulf1 (*66-68*), similarly shifts C&E
97 onset and suppresses *sumf1* and *sumf2* mutant phenotypes, indicating that heparan sulfate proteoglycans
98 (HSPGs) mediate C&E timing downstream of sulfatase modifiers. Together, these data support a model in
99 which *sumf2* expression at gastrulation onset reduces sulfatase activity, triggering a switch in HSPG sulfation
100 patterns to promote and/or permit C&E morphogenesis.
101
102 **RESULTS**
103
104 ***Ex vivo* convergence & extension requires new transcription at gastrulation onset**
105 Blocking transcription prior to ZGA prevents all gastrulation morphogenesis in zebrafish embryos (*54*).
106 However, it was not determined when new transcription is required for gastrulation cell movements nor the
107 specific genes that are required. We previously showed that otherwise naïve zebrafish embryonic explants
108 expressing Nodal signaling components recapitulate both C&E behaviors and their precise timing in culture,
109 while lacking other gastrulation movements (*36*), making them an ideal system to study C&E timing. To identify
110 the temporal window of gene expression required for C&E, we treated explants expressing the constitutively
111 active Nodal receptor Acvr1b* (also known as TARAM-A* (*69*)) with a time-course of the irreversible

transcription inhibitor Triptolide (*70*). We then assessed their ability to undergo C&E by measuring their extension when sibling embryos reached the 4-somite stage (12 hpf) (**Fig. 1A**). *acvr1b** explants treated when intact siblings reached 50% epiboly (5.3 hpf) failed entirely to extend, while those treated shortly thereafter at shield stage (6 hpf, gastrulation onset) or later were able to extend, albeit incompletely (**Fig. 1B, C**). To rule out the possibility that Triptolide interferes with C&E by disrupting Nodal signaling dynamics, we repeated the experiment by activating Nodal under two additional experimental conditions. First, we expressed the Nodal ligand Ndr2/Cyc in explants, which display delayed Nodal activation compared to *acvr1b** explants (*71*). Second, we expressed *acvr1b** in explants generated from Nodal signaling-deficient maternal-zygotic (MZ)*oep*-/- embryos (*72*), which exhibit continued signaling in the absence of feed-forward synthesis of new Nodal ligands. Both conditions responded identically to wildtype (WT) *acvr1b** explants, indicating that the requirement for transcription is independent of Nodal signaling *per se* (**Supplementary Fig. 1A, B, D, E**). This is consistent with Activin-induced *Xenopus* animal cap explants extending on time regardless of when in the competence window Activin was added (*38*). Finally, WT *acvr1b** explants treated with the reversible transcription inhibitor Flavopiridol (*73*) at 50% epiboly and washed out at 90% epiboly (5.3–9 hpf) similarly failed to extend (**Supplementary Fig. 1C, F**), demonstrating that the stage of inhibition, rather than its duration, was responsible for failed C&E. These results indicate that new gene expression starting at gastrulation onset is required for *ex vivo* C&E movements, independent of Nodal signaling dynamics.

sumf1 **and** ***sumf2*** **transcript levels invert at gastrulation onset**

Having established that transcription at gastrulation onset is crucial for C&E, we next identified genes whose expression is strongly upregulated during this time window. We previously profiled transcription in *ndr2, acvr1b*,* and uninjected control explants by bulk RNA sequencing at seven developmental stages spanning gastrulation (*71*) (**Fig. 1D**). We examined these data for candidate “trigger” genes whose expression exhibited a substantial increase between 50% epiboly and shield stage, corresponding to our experimentally determined transcriptional window. Because the timing of C&E onset is independent of Nodal signaling dynamics, we only considered genes with similar temporal expression profiles in explants of all three conditions, including uninjected controls. This analysis yielded a list of 180 genes, 129 of which had similar increasing expression profiles in intact zebrafish gastrulae (*74*) (**Supplementary Table 1A**). From these, we selected genes

140 exhibiting at least a 50% increase (Δ > 0.5x) in expression at gastrulation onset (shield stage) from their
141 baseline at 50% epiboly and whose expression at shield stage *in vivo* was over 5 transcripts per million,
142 producing a list of 28 genes (**Fig. 1E**) (**Supplementary Table 1B**). Because C&E begins simultaneously in
143 intact embryos and explants, we hypothesized these 28 genes represent candidates whose expression at
144 gastrulation onset may trigger C&E cell behaviors.

145 Among our candidate genes was *sulfatase modifying factor 2* (*sumf2*). *sumf2* encodes pFGE, a paralog
146 and antagonist of Formylglycine Generating Enzyme (FGE) (*65, 75*), encoded by *sulfatase modifying factor 1*
147 (*sumf1*). As its name implies, FGE converts cysteine residues to formylglycine, a rare but essential post-
148 translational modification required within the active site of all sulfatase enzymes for their activity (*75*).
149 Sulfatases catalyze the removal of sulfate groups from a variety of substrates, including lipids, steroids, and
150 glycosaminoglycans, modifying their biological activity (*76, 77*). Both pFGE (*sumf2*) and FGE (*sumf1*) are ER-
151 resident proteins that share high amino acid sequence similarity with the main distinction that pFGE lacks
152 enzymatic activity (*55, 75*). Evidence suggests that pFGE binds FGE alone or in complex with its sulfatase
153 substrates (*59, 65*), but it is not clear precisely how pFGE (*sumf2*) antagonizes FGE (*sumf1*) function. Although
154 other candidates exhibited more dramatic expression increases at gastrulation onset, we selected *sumf2* for
155 further study because its function during vertebrate development has never been explored, and its intriguing
156 complementary temporal expression patterns with *sumf1* during gastrulation. In zebrafish embryos and
157 explants, *sumf1* is maternally expressed but exhibits a sharp reduction in transcript levels just prior to
158 gastrulation onset, coinciding with increased *sumf2 (74)* (**Fig. 1F, Supplementary Fig. 1G**). Because *sumf2*
159 and *sumf1* encode a negative and positive regulator of sulfatase activity, respectively, we hypothesized that
160 this peak in the *sumf2/sumf1* ratio at gastrulation onset (6hpf) (**Fig. 1G**) reduces sulfatase activity and thus
161 increases sulfation of their substrates to trigger C&E movements.

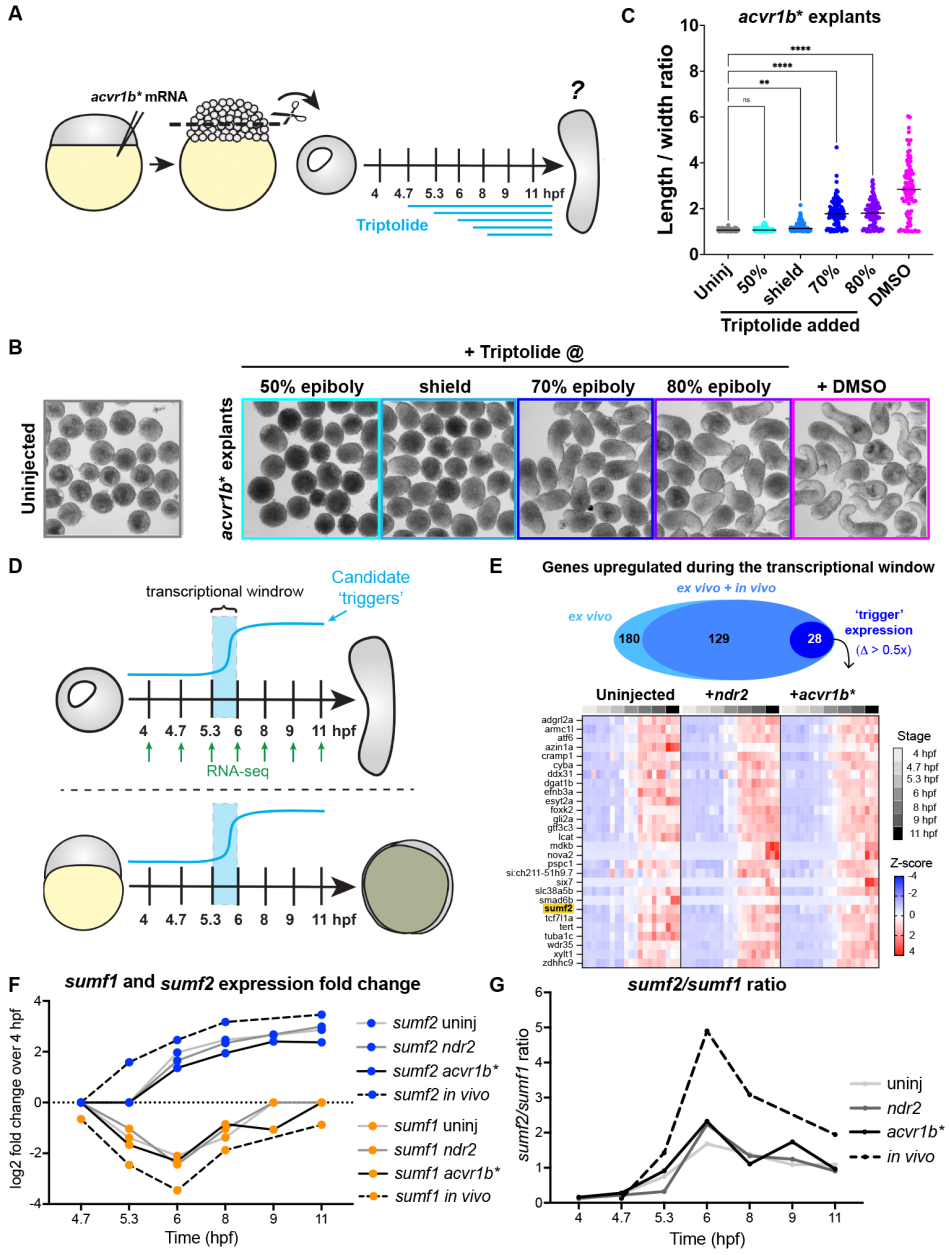

Fig. 1. *Ex vivo* convergence & extension requires new transcription at gastrulation onset. (A) Diagram of embryonic explants and Triptolide treatments (modified from (*36*)). **(B)** Representative images of uninjected and *acvr1b** explants at 12 hpf (equivalent of 4-somite stage) after treatment with triptolide at the indicated stages or with DMSO at 50% of epiboly. **(C)** Length/width ratios of explants shown in (B). Each dot represents a single explant from three independent trials, black bars are median values; p<0.0001, Mann-Whitney test. **(D)** Overview of comparisons between published bulk RNA-sequencing experiments from seven developmental stages in three explant conditions (uninjected, *acvr1b**, and *ndr2*) (top) and intact embryos (bottom). Candidate 'trigger' genes were strongly upregulated within the previously determined transcriptional window (5.3–6 hpf). **(E)** (Top) 180 genes exhibited 'trigger' expression patterns in all explant conditions (light blue); of these, 129 were also upregulated in intact embryos (blue), and 28 showed a sharp increase (Δ > 0.5x) with significant expression levels (>5 TPM, dark blue). (Bottom) Heatmap of candidate 'trigger' genes in uninjected, *acvr1b**, and *ndr2* explants. *sumf2* (highlighted in yellow) was selected for further study. **(F)** Fold-change expression of *sumf1* and *sumf2* transcripts over 4 hpf in explants (solid lines) and embryos (dashed lines) over time. **(G)** *sumf2/sumf1* expression ratio in explants (solid line) and embryos (dashed line) over time. Note the peak in the *sumf2/sumf1* ratio at 6 hpf, coinciding with the previously determined transcriptional window.

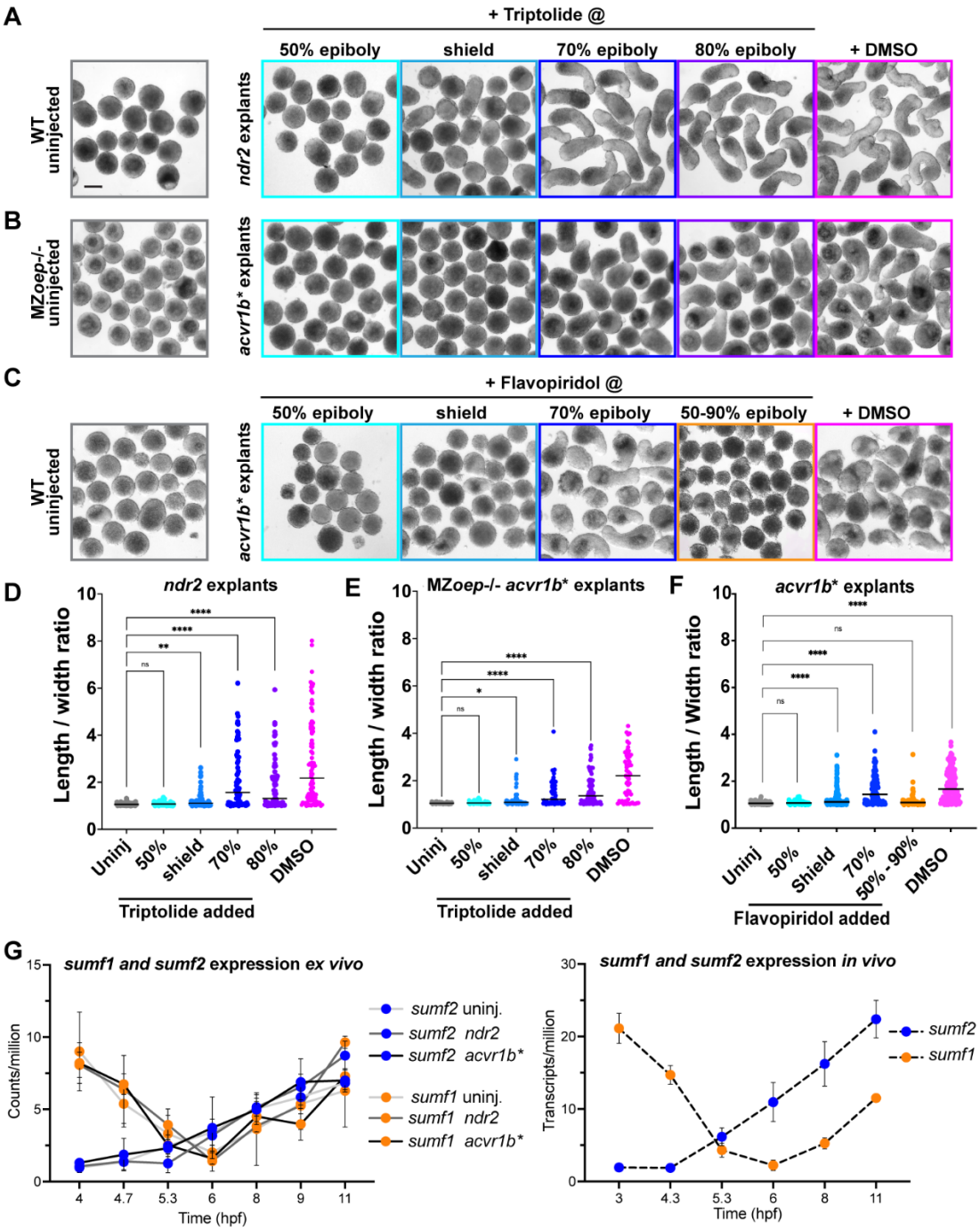

Supplementary Fig. 1. *Ex vivo* convergence & extension requires new gene expression at gastrulation onset independently of Nodal signaling dynamics. **(A, B)** Representative images of WT uninjected and *ndr2* explants (A), or MZ*oep*-/- uninjected and *acvr1b** explants (B) at 12 hpf (equivalent of 4-somite stage) after treatment with triptolide at the indicated stages or with DMSO at 50% of epiboly. Scale bar 200 μm. **(C)** Representative images of WT uninjected and *acvr1b** explants at 12 hpf (equivalent of 4-somite stage) after treatment with reversible transcription inhibitor Flavopiridol at the indicated stages or with DMSO at 50% of epiboly. **(D-F)** Length/width ratios of explants shown in (A, B and C), respectively. Each dot represents a single explant from three independent trials, black bars are median values; $p<0.0001$, Mann-Whitney test. **(G)** Expression levels of *sumf1* and *sumf2* in uninjected (light grey lines), *ndr2* (grey lines) and *acvr1b** (black lines) explants (left), and embryos (dashed lines, right) over time. Dots represent the mean of three (for explants) or five (for embryos) bulk RNA-seq replicates and error bars represent standard deviation.

192

193 **Excess or loss of sulfatase modifying factors causes C&E defects in zebrafish gastrulae**

194 To investigate the role of sulfatase modifying factors in C&E morphogenesis, we employed both gain- and
195 loss-of-function approaches and performed morphometric analysis at the end of gastrulation (tailbud stage, 10
196 hpf). We first overexpressed *sumf1* or *sumf2* by mRNA injection into single-cell WT embryos. *sumf1*
197 overexpressing (OE) gastrulae exhibited a significant reduction in anteroposterior (AP) axis length and wider
198 notochords, characteristic of C&E defects, and *sumf2* OE embryos showed similar but milder phenotypes (**Fig.**
199 **2**). Next, we examined gastrulae of the recently characterized *sumf1*^{la015919Tg} mutant line (hereafter *sumf1*-/-)
200 harboring a viral insertion in exon 1 that abolishes FGE activity (*78*). Homozygous mutant embryos survived to
201 adulthood (*78*), enabling examination of MZ*sumf1*-/- gastrulae, which also exhibited reduced AP axis length
202 and wider notochords indicative of impaired C&E (**Fig. 2**). Because no existing *sumf2* mutant line was
203 available, we used CRISPR to generate a 7 bp insertion in exon 2 of *sumf2* (named *bcm126*), resulting in a
204 premature stop codon (**Supplementary Fig. 2A**). Homozygous *sumf2*$^{bcm126/bcm126}$ embryos (hereafter *sumf2*-/-),
205 showed a substantial reduction in *sumf2* transcript levels by qRT-PCR (**Supplementary Fig. 2C**), confirming
206 this as a strong loss-of-function allele. These mutants also survived to adulthood, enabling us to maintain the
207 line as homozygotes and analyze MZ*sumf2*-/- embryos. Notably, approximately 10% of MZ*sumf2*-/- larvae
208 displayed a tail-curled-up phenotype at 48 hpf and a variable number of *sumf2*-/- adults were undersized and
209 scoliotic (**Supplementary Fig. 2D, E**). Although MZ*sumf2*-/- mutant gastrulae did not exhibit C&E defects,
210 *sumf1* OE in this background produced more severe C&E phenotypes than in WT embryos (**Figure 2**),
211 supporting an antagonistic role for *sumf2*/pFGE on *sumf1*/FGE. Together, these results demonstrate that
212 altering levels of *sumf1* or/and *sumf2* disrupts C&E gastrulation morphogenesis *in vivo*.

213

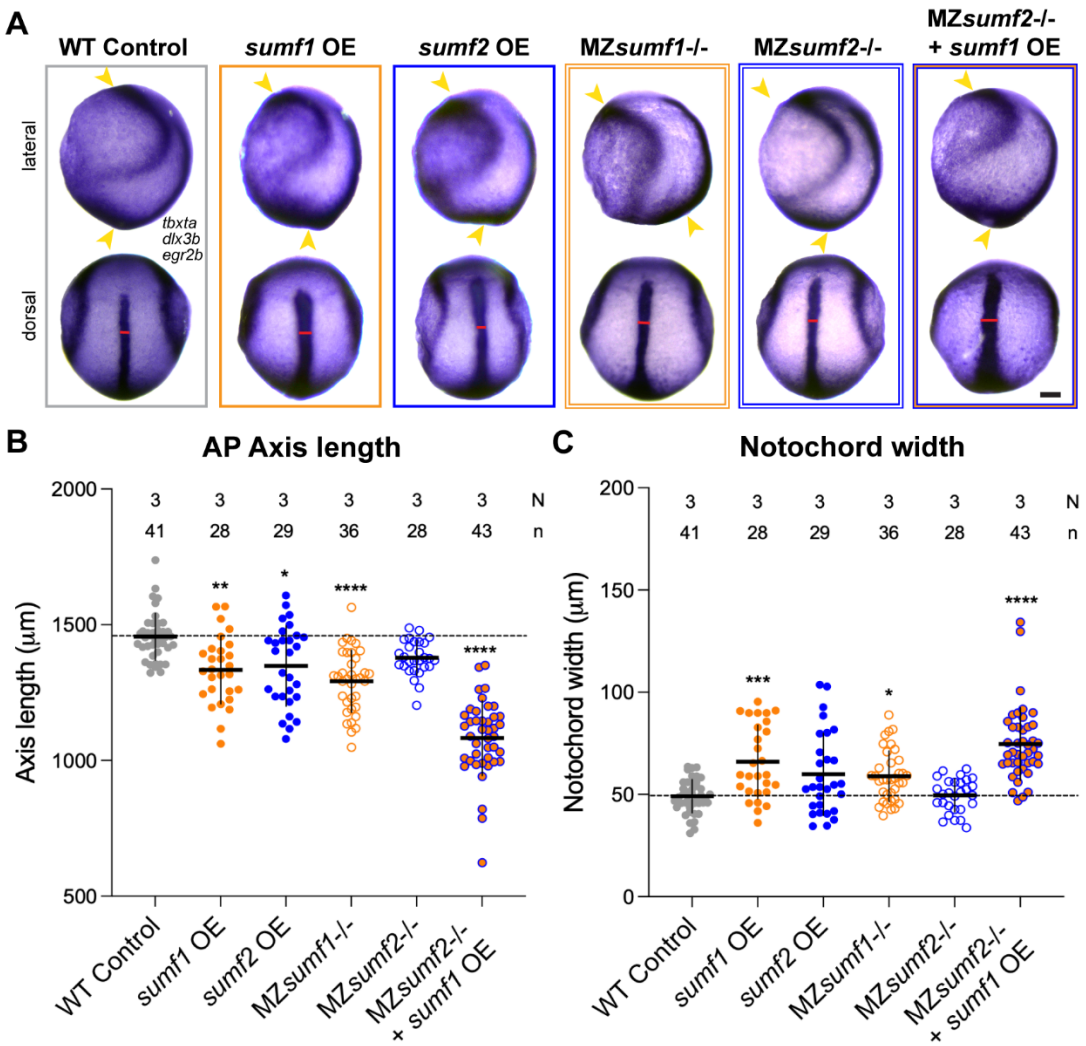

Fig. 2. C&E defects in zebrafish gastrulae with altered sulfatases modifiers factor levels.
(A) Representative images of whole mount in situ hybridization (WISH) for *tbxta* (mesoderm), *dlx3b* (neural plate border) and *egr2b* (rhombomeres 3 & 5) in tailbud stage (10 hpf) embryos of the indicated conditions. Anterior is up in all images, lateral views are shown on top, dorsal views on bottom. Scale bar 100 µm. **(B, C)** Anteroposterior (AP) axis length (B, yellow arrowheads) and notochord width (C, red lines) of embryos depicted in (A). Each dot represents a single embryo, N: number of independent experiments, n: number of embryos. Means and standard deviation are indicated; * $p<0.05$, ** $p<0.01$, **** $p<0.0001$ compared to WT control group by Kruskal–Wallis and Dunn's multiple comparisons tests.

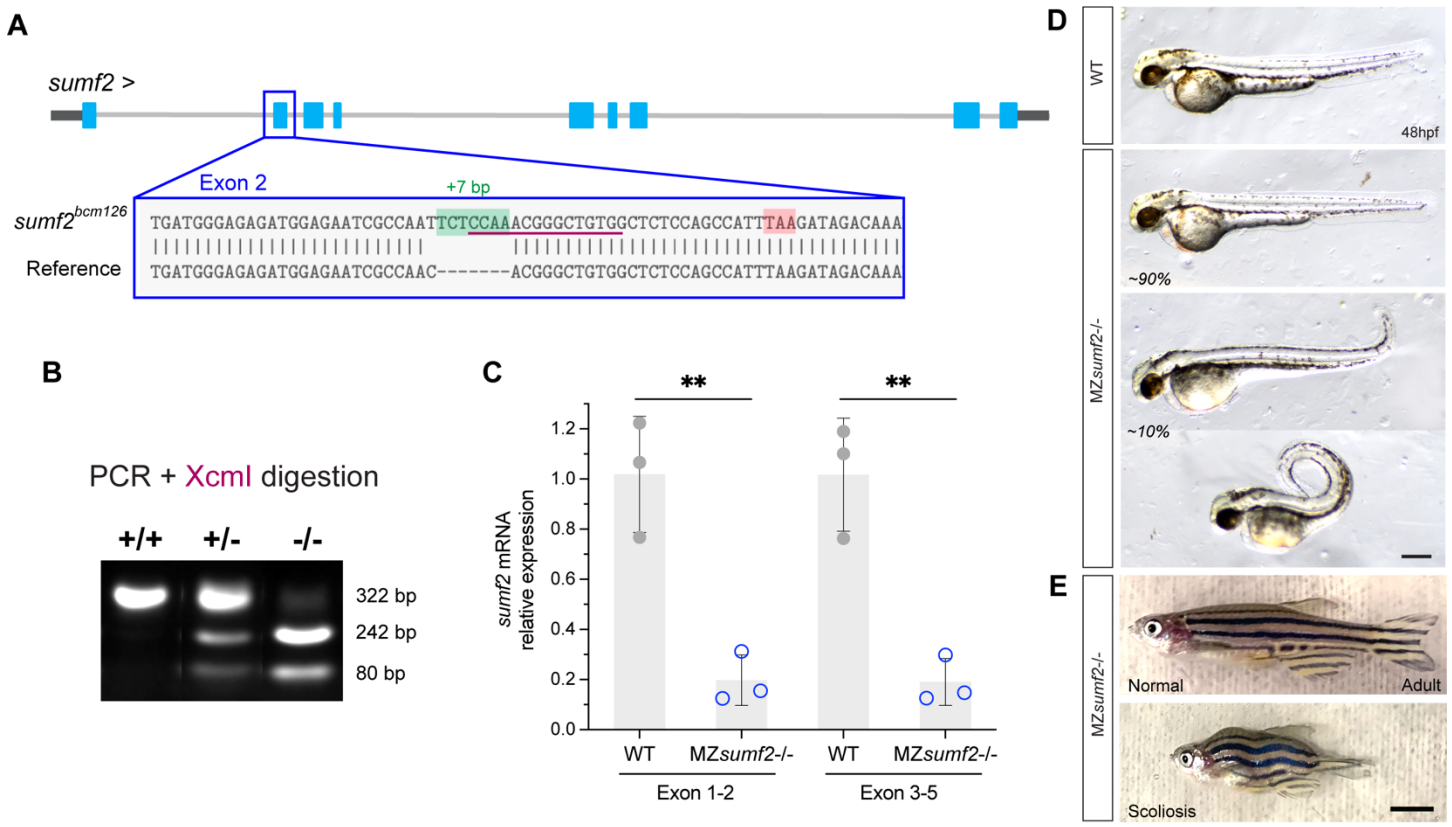

Supplementary Fig. 2. Characterization and genotyping of new *sumf2* loss-of-function allele. (A) Diagram of CRISPR-induced 7 bp insertion (green) in exon 2 of *sumf2* (*sumf2*^{bcm126}), resulting in a premature stop codon (red). **(B)** The *sumf2*^{bcm126} allele creates an XcmI restriction site (purple underline in (A)), enabling genotyping by digestion of a 322 bp PCR-amplified fragment, which yields 242 bp and 80 bp products in heterozygous (+/−), and homozygous (−/−) but not WT (+/+) samples. **(C)** Relative expression of *sumf2* transcripts in WT and MZ*sumf2*-/- larvae, measured by RT-qPCR using primers spanning *sumf2* exon 1–2 and exon 3–5. Means and standard deviation are indicated. Each dot represents one of three independent clutches; ** $p<0.01$, Mann-Whitney test. **(D)** Representative images of WT and MZ*sumf2*-/- larvae at 48 hpf. Approximately 90% of MZ*sumf2*-/- larvae developed normally, while ~10% displayed varying degrees of tail-curled-up phenotypes. Anterior is to the left; scale bar 200 μm. **(E)** Representative images of MZ*sumf2*-/- adult fish showing *Normal* and *Scoliosis* phenotypes. Scale bar 500 μm.

237 ***sumf1* and *sum2* levels modify the timing of C&E *ex vivo***

238 Next, we examined the effects of altered *sumf1* and *sumf2* levels in zebrafish embryonic explants, in which
239 C&E is isolated from other concurrent morphogenetic processes. Surprisingly, neither OE nor deficiency of
240 *sumf1* or *sumf2* impaired the extension of *acvr1b** explants at the equivalent of 4-somite stage
241 (**Supplementary Fig. 3**), indicating that they are dispensable for C&E *per se*. To assess whether *sumf1* or
242 *sumf2* levels instead influenced the timing of C&E morphogenesis, we acquired time-lapse recordings of
243 *acvr1b** explants to precisely determine the onset of morphological extension. Extension onset was defined as
244 the time point when a visible tip first emerged from an initially round explant (**Fig. 3A**). Importantly, all explants
245 were staged relative to blastopore closure in age-matched intact embryos of the same genetic background
246 mounted in the same dish. As previously described (*36*), WT *acvr1b** explants (WT control) and controls co-
247 injected with *superfold-GFP* mRNA (*sf-GFP* OE) initiated extension around 8hpf. Strikingly, extension began
248 significantly later upon *sumf1* OE and significantly earlier upon *sumf2* OE (**Fig. 3B**). Co-overexpression of
249 *sumf1* and *sumf2* restored the normal time of extension onset (**Fig. 3B**), demonstrating that the balance
250 between these factors (rather than their absolute levels) determines the time of C&E onset. In the converse
251 loss-of-function experiments, we found that extension onset was precocious in MZ*sumf1*-/- explants and
252 delayed in MZ*sumf2*-/- explants (**Fig. 3A, B**), consistent with - but opposite to - *sumf1* and *sumf2* OE
253 phenotypes. MZ*sumf1*-/-, MZ*sumf2*-/- double mutant explants phenocopied the precocious extension of
254 MZ*sumf1*-/- single mutants, consistent with *sumf2/*pFGE modulating C&E timing via its role as an antagonist of
255 *sumf1*/FGE. Together, these results demonstrate that the ratio of *sumf1/sumf2* governs the timing of explant
256 extension, with higher *sumf1* delaying and higher *sumf2* advancing C&E onset.

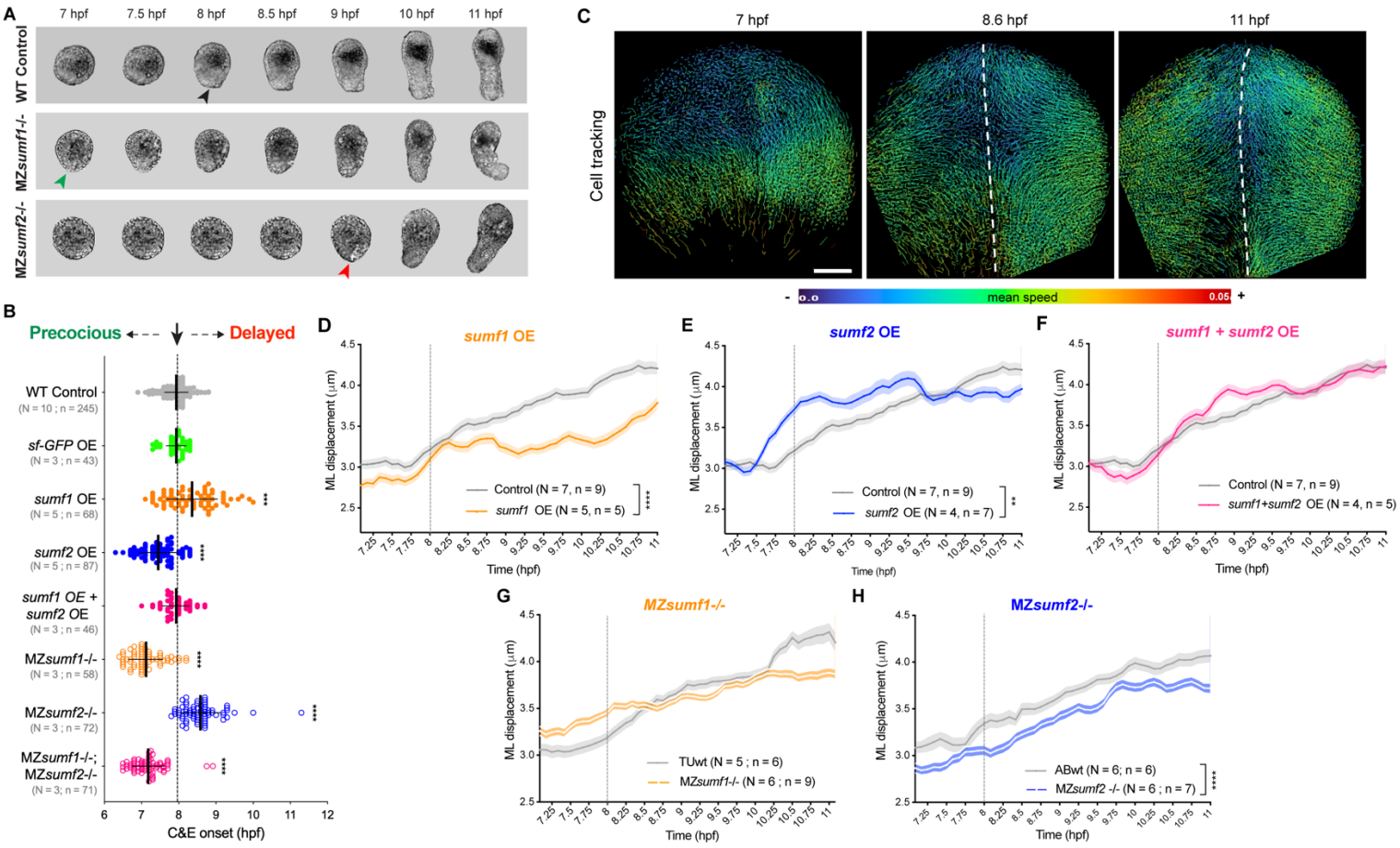

Fig. 3. *sumf1* and *sum2* levels control the timing of C&E. (A) Representative bright-field images of *acvr1b** explants of the indicated genotype over time. Black, red, and green arrowheads indicate timely, precocious, and delayed onset of extension, respectively. **(B)** Onset of extension in *acvr1b** explants of the indicated conditions. Dotted line shows typical extension onset of WT control explants around 8 hpf. Each dot represents a single explant. Means and standard deviation are indicated, N: number of independent experiments, n: number of explants, *** p<0.001, **** p<0.0001 compared with WT control group by Kruskal–Wallis and Dunn's multiple comparisons tests. **(C)** Representative images of automated nuclear tracking in the dorsal hemisphere of zebrafish gastrulae, starting before C&E onset (7 hpf). Tracks are color-coded by mean speed; dashed lines mark the dorsal midline; scale bar 100 μm. **(D-H)** ML cell displacement over time for WT control (gray lines) and *sumf1* OE (D), *sumf2* OE (E), *sumf1* + *sumf2* OE (F), MZ*sumf1*-/- (G), and MZ*sumf2*-/- (H) embryos. Dotted line shows typical onset of convergence movements in WT control embryos around 8 hpf. Means and standard error are indicated, N: number of independent experiments, n: number of embryos. ** p<0.01, **** p<0.0001 compared with WT control group by Wilcoxon signed-rank test.

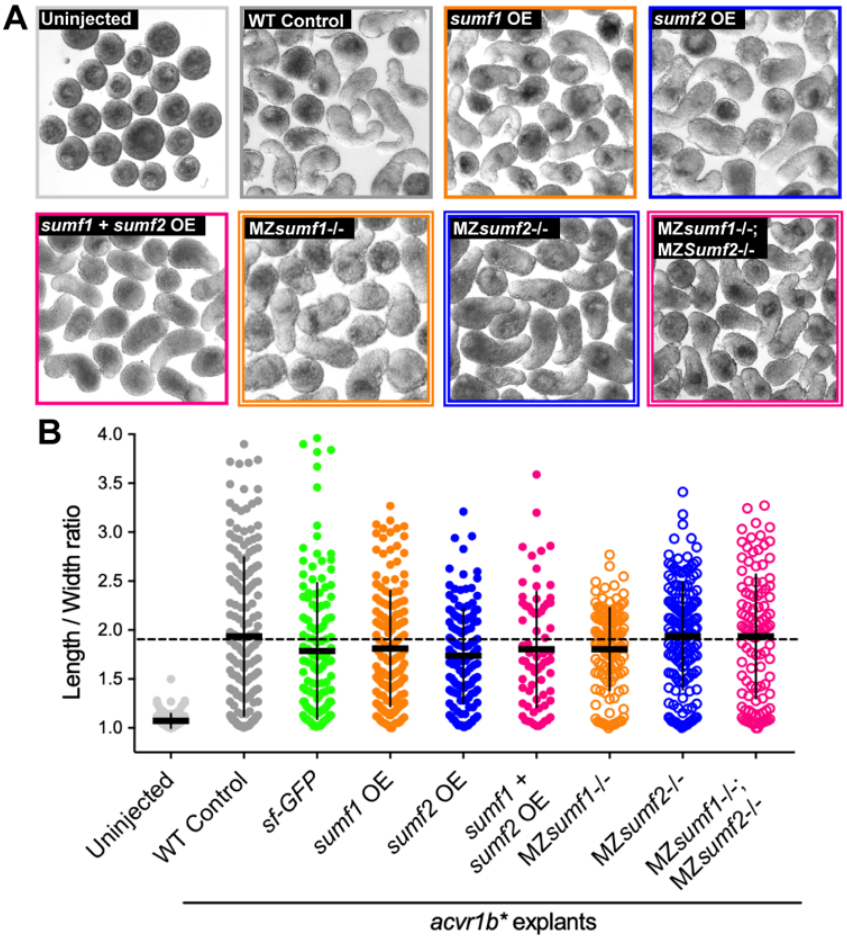

Supplementary Fig. 3. Altered *sumf1* and *sumf2* levels do not impair extension of Nodal-induced explants. (A) Representative images of uninjected and *acvr1b** explants from the indicated experimental conditions. **(B)** Length/width ratios of explants at the equivalent of 4-somite stage (12 hpf) shown in (A). Each dot represents a single explant from three independent trials. Means and standard deviation are indicated. $p>0.05$, Kruskal–Wallis test.

282 ***sumf1* and *sum2* levels modify the timing of C&E *in vivo***

283 To determine whether *sumf1* and *sumf2* similarly modify the timing of C&E cell movements *in vivo*, we
284 acquired confocal time-lapse movies of *H2B-scarlet*-labeled gastrulae from 6.5 – 11 hpf and performed
285 automated nuclear tracking (see *Methods*; **Fig. 3C**). To ensure accurate stage matching across experiments,
286 all embryos were staged relative to formation of the second somite, which was readily visible at the end of
287 each movie. Convergence movements were quantified as the mediolateral (ML) displacement of dorsal and
288 lateral cells over time (**Fig. 3D–H**). Because convergence movements are reduced within the embryonic
289 midline where extension is more prominent (*79*), cells within 100 μm of the dorsal midline were excluded from
290 our analysis. In WT control embryos, we observed an upward inflection of ML displacement beginning around
291 7.75 - 8 hpf, marking the onset of convergence movements (consistent with previous findings (*18, 19*)), which
292 continued to increase gradually thereafter (**Fig. 3D–H**). Upon *sumf1* OE, baseline convergence speed was
293 reduced and, although convergence movements began at the same time as controls, they remained
294 substantially slower (**Fig. 3D)**. *sumf2* OE embryos, on the other hand, had similar baseline convergence
295 speeds as controls but with an earlier inflection point (**Fig. 3E)**. For much of gastrulation, these movements
296 were also faster than those of controls, indicating a likely change in both onset and pace of convergence
297 movements. As in explants, co-OE of both *sumf1* and *sumf2* restored convergence movements to control
298 timing and speeds (**Fig. 3F)**. Also as in explants, *in vivo* cell tracking of MZ*sumf1-/-* and MZ*sumf2-/-* mutants
299 revealed opposite effects to their overexpression. Convergence onset in MZ*sumf1*-/- embryos trended earlier
300 than controls and baseline speed trended higher, although these movements plateaued later in gastrulation
301 (**Figure 3G)**. Conversely, baseline convergence in MZ*sumf2-/-* mutants was slower than controls with a later
302 inflection point, indicating delayed convergence (**Fig. 3H)**. Together with our *ex vivo* results, these data support
303 a model in which *sumf2*/pFGE counters the activity of *sumf1*/FGE to control the onset and pace of C&E cell
304 movements during gastrulation.
305

306 **Sulfatase modifiers govern C&E via the extracellular sulfatase Sulf1**

307 Because *sumf1*/FGE and *sumf2*/pFGE together regulate sulfatase activity levels, we hypothesized that
308 high *sumf2/sumf1* ratios trigger C&E onset by reducing the activity of one or more key sulfatases. Indeed,
309 increased sulfatase activity was shown to disrupt gastrulation morphogenesis in *Xenopus* and sea urchin (*64,*
310 *80-83*). The zebrafish genome encodes 17 sulfatases, 11 of which are expressed during peri-gastrulation
311 stages (*74*) (**Supplementary Fig. 4A**). To identify which of these mediates the effect of *sumf1/sumf2* on C&E
312 timing, we overexpressed each of these 11 sulfatases and performed morphometric analysis at tailbud stage
313 and scored axis phenotypes at 24 hpf. Notably, three of them — the heparan sulfate endosulfatases *sulf1* and
314 *sulf2a*, and the chondroitin sulfatase *arsb* — produced severe AP axis extension defects and increased
315 notochord width, consistent with C&E defects (**Supplementary Fig. 4B-E**). Unlike *sumf1* and *sumf2* OE,
316 overexpression of these three sulfatases also prevented full extension of *acvr1b** explants at the equivalent of
317 4-somite stage (**Supplementary Fig. 4F, G**). However, only *sulf1* OE significantly delayed *acvr1b** explant
318 extension, while the other two had no effect on C&E timing (**Fig. 4A**). Thus, of the 17 zebrafish sulfatases, only
319 Sulf1 was found to affect both C&E morphogenesis and its timing.

320 To further investigate the role of Sulf1 in zebrafish gastrulation morphogenesis, we examined C&E in
321 MZ*sulf1*$^{sjr9/sjr9}$ full-locus deletion mutants (Kaur Bajwa et al, in submission) (hereafter MZ*sulf1-/-*). MZs*ulf1-/-*
322 embryos exhibited reduced AP axis length at tailbud stage (**Fig. 4B-D)** and MZs*ulf1-/- acvr1b** explants
323 showed impaired extension (**Supplementary Fig. 4F-G)**, indicating that both gain and loss of Sulf1 reduces
324 C&E. Strikingly, MZ*sulf1-/- acvr1b** explants exhibited precocious extension (**Fig. 4A**), similar to MZ*sumf1-/-*
325 and *sumf2* OE explants (but opposite to *sulf1* OE). We next quantified the effect of Sulf1 levels on C&E onset
326 *in vivo*. Convergence speed was drastically reduced upon *sulf1* OE (**Fig. 4E**) while MZ*sulf1-/-* gastrulae
327 exhibited earlier and enhanced convergence movements compared to WT controls (**Fig. 4F**). These results
328 highlight Sulf1 as a strong candidate for the key sulfatase controlling C&E onset.

329 To examine the relationship between Sulf1 and *sumf1*/FGE, we generated *acvr1b** explants co-injected
330 with low doses of each mRNA alone or in combination. The combination of otherwise sub-phenotypic doses of
331 *sumf1* and *sulf1* synergistically delayed and reduced explant extension (**Fig. 4G, Supplementary Fig. 4F, G),**
332 consistent with *sumf1*/FGE enhancing Sulf1 activity. Finally, we tested whether *sumf1* OE could delay explant
333 extension in the absence of *sulf1*. We found that although *sumf1* OE significantly delayed extension onset in

334 WT explants, it had no effect on the onset of extension in MZ*sulf1*-/- explants, which remained precocious (**Fig.**
335 **4G)**. Together, these results implicate Sulf1 as the primary sulfatase through which *sumf1*/FGE and
336 *sumf2*/pFGE govern the timing of C&E morphogenesis.
337

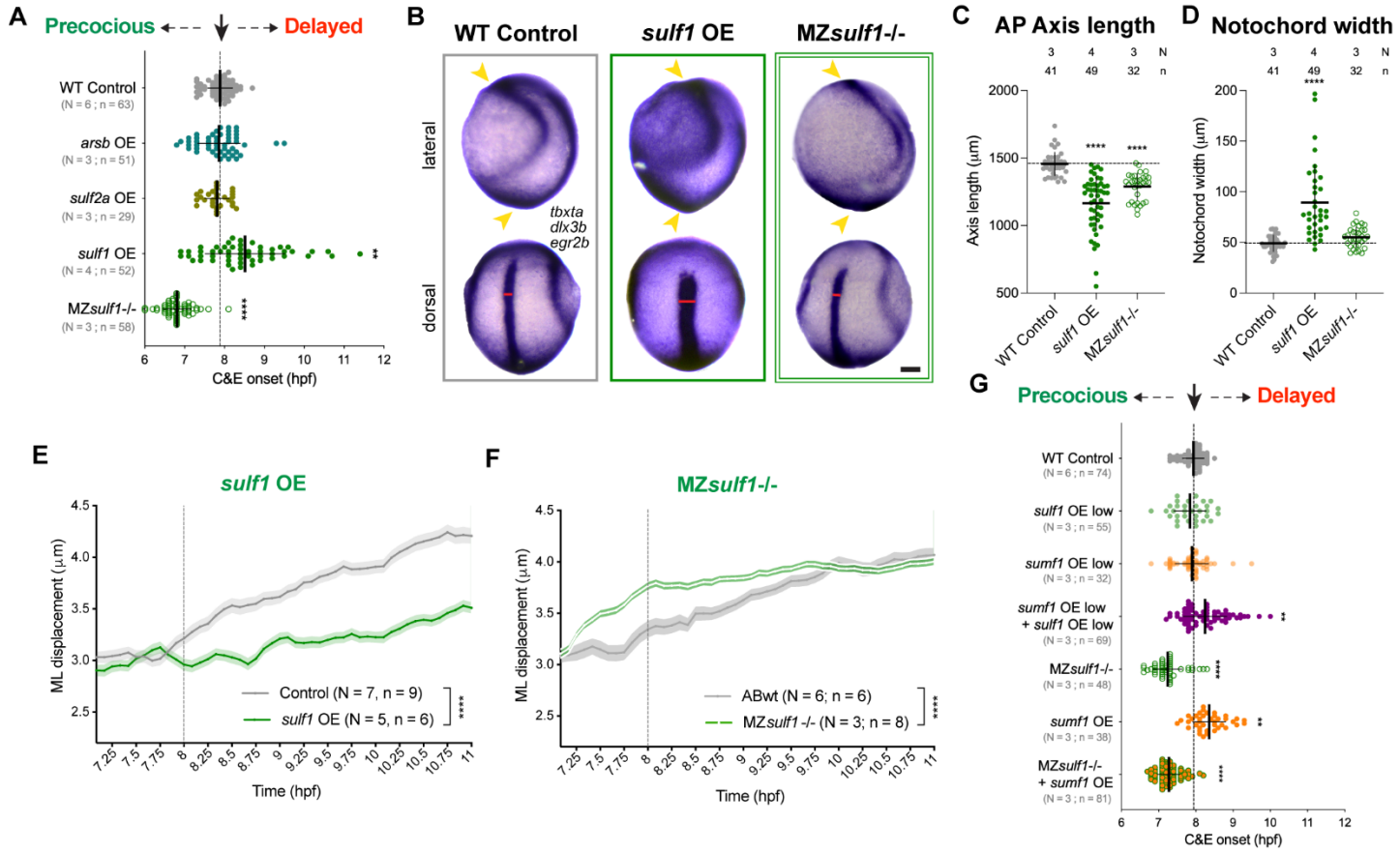

338

339 **Fig. 4. The extracellular sulfatase Sulf1 governs C&E and its timing. (A)** Onset of extension in *acvr1b**
340 explants of the indicated conditions. Dotted line shows typical extension onset of WT control explants around 8
341 hpf. Each dot represents a single explant. Means and standard deviation are indicated, N: number of
342 independent experiments, n: number of explants. *** p<0.001, **** p<0.0001 compared with WT control group
343 by Kruskal–Wallis and Dunn's multiple comparisons tests. **(B)** Representative images of WISH for *tbxta*
344 (mesoderm), *dlx3b* (neural plate border) and *egr2b* (rhombomeres 3 & 5) in tailbud stage (10 hpf) embryos of
345 the indicated conditions. Anterior is up in all images, lateral views are on top, dorsal views on bottom. Scale bar
346 100 µm. **(C, D)** Anteroposterior (AP) axis length (C) and Notochord width (D) were quantified as in Figure 2
347 from embryos depicted in (B). Each dot represents a single embryo. Means and standard deviation are
348 indicated. **** p<0.0001 compared with WT control group by Kruskal–Wallis and Dunn's multiple comparisons
349 tests. **(E, F)** ML cell displacement from automated nuclear tracking (as in Figure 3) in WT control, *sulf1* OE (E)
350 and MZ*sulf1*-/- (F) zebrafish gastrulae. Means and standard error are indicated. N: number of independent
351 experiments, n: number of embryos. **** p<0.0001 compared with WT control group by Wilcoxon signed-rank
352 test. **(G)** Onset of extension in *acvr1b** explants of the indicated conditions. Dotted line shows typical extension
353 onset of WT control explants around 8 hpf. Each dot represents a single explant. Means and standard
354 deviation are indicated, N: number of independent experiments, n: number of explants. ** p<0.01, ****
355 p<0.0001 compared with WT control group by Kruskal–Wallis and Dunn's multiple comparisons tests.
356

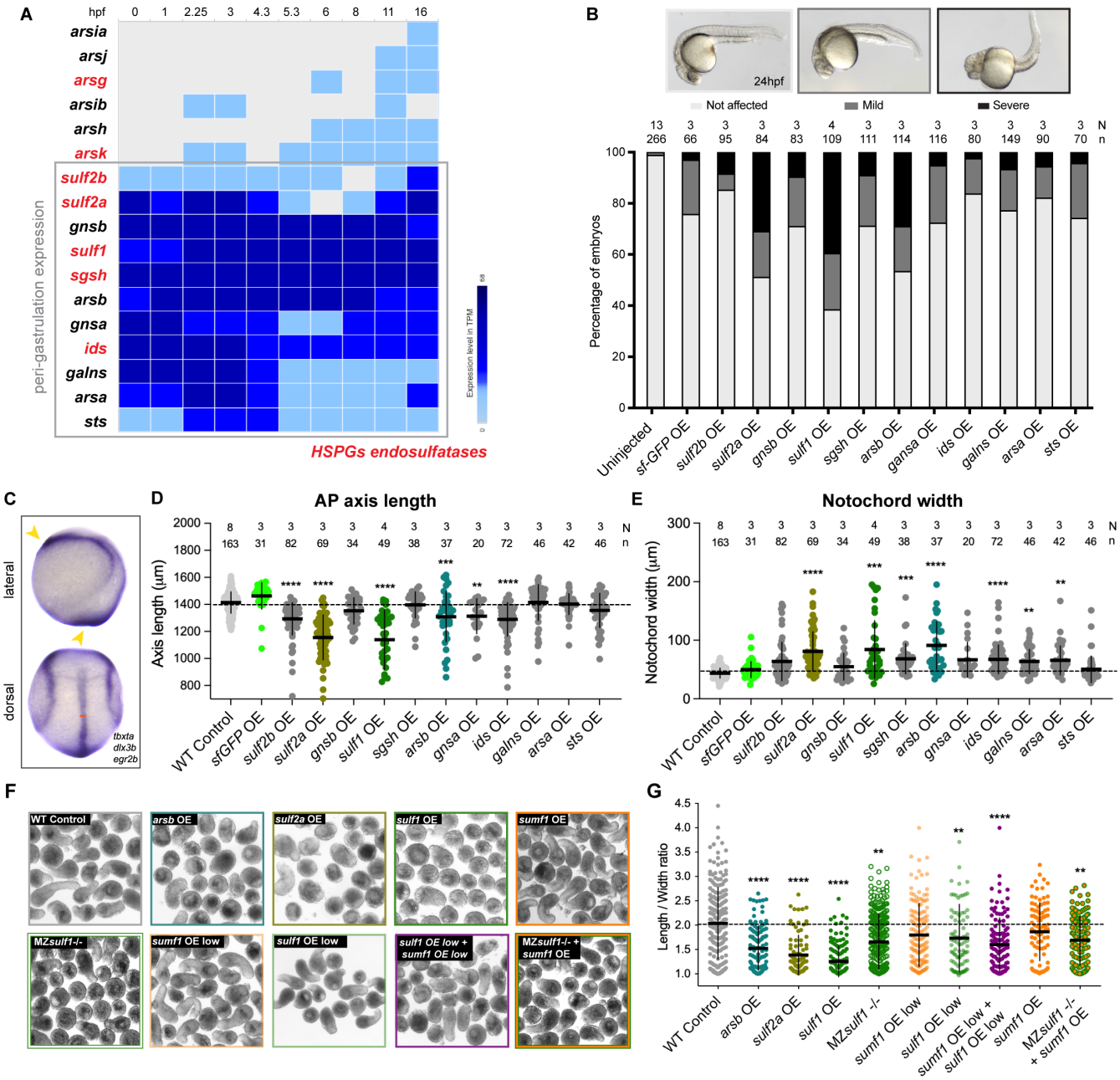

Supplementary Fig. 4. Evaluation of C&E defects upon sulfatase overexpression. (A) Expression levels of all 17 zebrafish sulfatases over time based on publicly available bulk RNA-seq data. Gray square indicates the 11 expressed during peri-gastrulation, HSPG endosulfatases are in red. **(B)** (Top) Representative images of 24 hpf embryos overexpressing each of the 11 peri-gastrulation sulfatases displaying a range of axis phenotypes scored as *"Not affected"*, *"Mild"* or *"Severe"*. (Bottom) Mean percentage of 24 hpf embryos of the conditions indicated exhibiting each class of axis defect. N: number of independent experiments, n: number of embryos. **(C)** WISH for *tbxta* (mesoderm), *dlx3b* (neural border) and *egr2b* (rhombomeres 3 & 5) in tailbud stage (10 hpf) embryos shown from lateral (top) and dorsal (bottom) views. **(D, E)** Anteroposterior (AP) axis length (D) and Notochord width (E) (as in Figure 2) in control and sulfatase-overexpressing embryos. Each dot represents a single embryo. Means and standard deviation are indicated. ** $p<0.01$, *** $p<0.001$, **** $p<0.0001$ as compared with WT control group by Kruskal–Wallis and Dunn's multiple comparisons tests. **(F)** Representative images of *acvr1b** explants from the indicated experimental conditions. **(G)** Length/width ratios of 12 hpf explants shown in (F). Each dot represents a single explant. Means and standard deviation are indicated. * $p>0.05$, ** $p<0.01$, **** $p<0.0001$ compared with WT control group by Kruskal–Wallis and Dunn's multiple comparisons tests.

373 **Sulfated heparan sulfate proteoglycans increase with C&E onset**

374 Sulf1 is an extracellular sulfatase that removes 6-*O* sulfation from GlcA-GlcNS6S (D0S6) and IdoA2S-
375 GlcNS6S (D2S6) disaccharide units of heparan sulfate proteoglycans (HSPGs)(*67*). We would therefore
376 expect the inversion of *sumf1*/FGE and *sumf2*/pFGE levels at the beginning of gastrulation to decrease Sulf1
377 activity, leading to increased sulfated HSPG levels at late gastrulation. Indeed, Alcian Blue staining (at pH ~1)
378 (*84*) for overall glycosaminoglycan (GAG) sulfation increased dramatically from early (50% epiboly) to late
379 (90% epiboly) gastrulation stages, indicating increased embryo-wide GAG sulfation. Treatment with sodium
380 chlorate, which prevents the formation of the sulfate donor 3'-phosphoadenosine 5'-phosphosulfate (PAPS)
381 (*85, 86*), drastically diminished Alcian Blue staining (**Fig. 5A**), confirming its specificity.

382 Because Alcian Blue stains all negatively charged GAGs, we next quantified levels of sulfated heparan
383 sulfate (HS) disaccharides by hydrophilic interaction liquid chromatography with mass spectrometry (HILIC-
384 LC/MS) in early and late zebrafish gastrulae (*87*). We found that total HS levels increased significantly between
385 50% and 80% epiboly stages (**Fig. 5B**). Although we observed no changes in the percentage of the 6-*O*
386 sulfated D0S6 and D2S6 disaccharides between stages (**Fig. 5C**), we did find a significant increase in total
387 levels of these 6-*O* sulfated disaccharides at late gastrulation (reflecting the observed increase in total HS
388 levels) (**Fig. 5D**). These results indicate that sulfation of Sulf1 substrates increases during gastrulation,
389 consistent with our hypothesis that the peak *sumf2/sumf1* ratio at gastrulation onset leads to reduced Sulf1
390 activity.

391

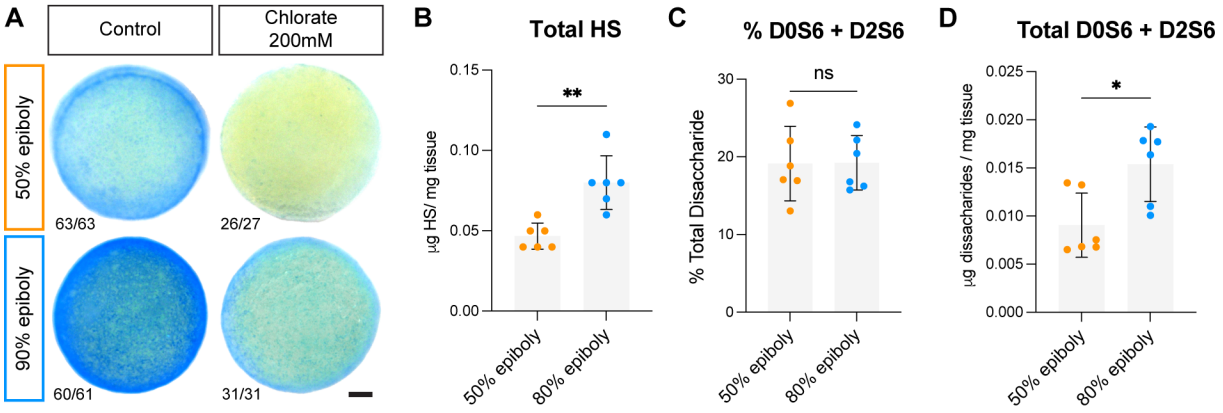

Fig. 5. Heparan sulfate proteoglycans and their sulfation increase during gastrulation. (A) Representative images of zebrafish early (50% epiboly, 5.3 hpf) and late (90% epiboly, 9 hpf) gastrulae stained with Alcian Blue for sulfated GAGs. Alcian Blue staining was diminished in zebrafish embryos treated at dome stage (4.3 hpf) with 200 mM sodium chlorate. Fractions indicate the number of embryos with the depicted staining pattern over number of embryos examined. Scale bar 100 μm. **(B-D)** HILIC-LC/MS analysis of early and late zebrafish gastrulae showing the total amount of heparan sulfate (HS) (B), the percentage of the D0S6 and D2S6 disaccharides (C), and the total amount of D0S6 and D2S6 disaccharides (D) at the stages indicated. Plots show mean and standard deviation, with each dot representing an independent clutch of 50 embryos, ** $p<0.01$, * $p< 0.05$, Mann-Whitney test.

404 **HSPGs mediate the effects of sulfatase modifiers on C&E timing**

405 Sulfatases modify a large number of biological substrates, including lipids, steroids, and multiple GAGs
406 (*88*). To test whether sulfated HSPGs influence C&E morphogenesis and its timing, we experimentally
407 decreased and increased sulfated HS levels within embryos and explants. To inhibit overall sulfation, including
408 GAGs, we treated dome stage embryos (4.3 hpf) with two different doses of sodium chlorate (200 mM and 50
409 mM), which we previously showed reduced Alcian Blue staining in zebrafish gastrulae (**Fig. 5A**). We observed
410 severe AP axis shortening and cyclopia in 24 hpf embryos treated with the higher dose, and milder axis defects
411 at the lower dose (**Fig. 6A**). A dose-dependent effect on C&E was also observed at tailbud stage (**Fig. 6B-D**),
412 demonstrating that sulfation is required for proper C&E morphogenesis (as previously reported (*89-91*)).
413 Although explants treated with the higher dose were not viable, treatment with the lower dose of sodium
414 chlorate also dramatically reduced extension of *acvr1b∗* explants (**Supplementary Fig. 5A, B**). Sodium
415 chlorate treatment also significantly delayed extension onset in both WT control and, importantly, in MZ*sumf1*-
416 /- explants in which extension otherwise occurred early (**Fig. 6E**, **Supplementary Fig. 5C**). This finding
417 strongly suggests that loss of *sumf1* induces precocious C&E by enhancing sulfation.

418 In a complementary experiment, we increased levels of sulfated HS by injecting the extracellular space of
419 256-cell stage embryos with 10 ng/ml HS (or water as a control) (**Fig. 6F**). As previously reported (*92*), HS-
420 injected embryos exhibited dorsalized phenotypes (**Supplementary Fig. 5D**), likely reflecting increased FGF
421 signaling (*93*). Notably, while increased HS did not affect the extension of *acvr1b∗* explants at the equivalent of
422 4-somite stage (**Supplementary Fig. 5A, B**), their extension onset was significantly earlier than control
423 explants (**Fig. 6G, Supplementary Fig. 5E**). HS injection also advanced extension onset in MZ*sumf2*-/-
424 explants (**Fig. 6G, Supplementary Fig. 5E**), indicating that increased HS levels are sufficient to trigger
425 precocious C&E *ex vivo* and can override the delay caused by *sumf2* deficiency. Taken together, these results
426 support a model in which *sumf2* expression at gastrulation triggers the timely onset of C&E cell movements by
427 reducing Sulf1 activity and consequently increasing sulfation of HSPGs.

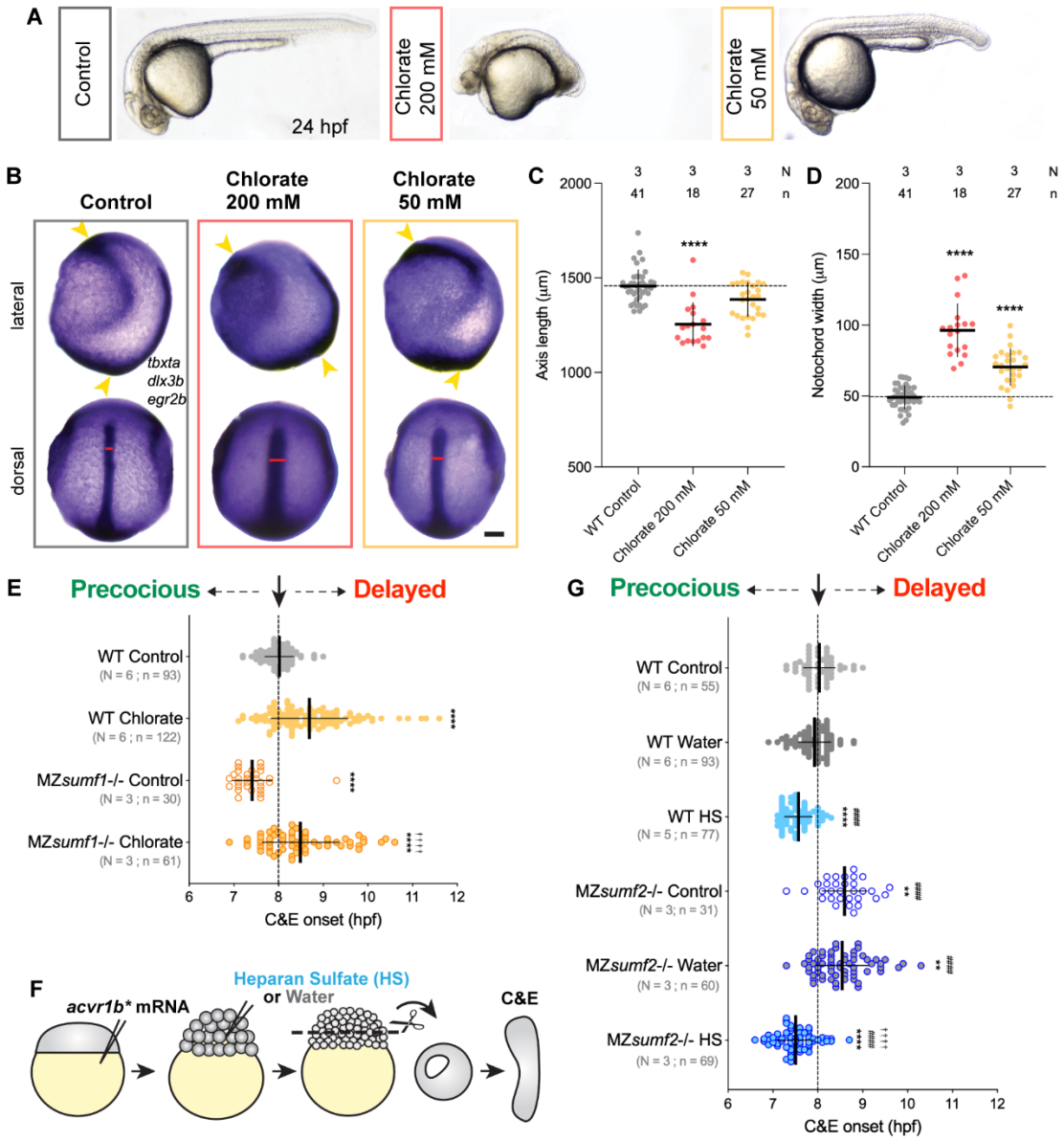

Fig. 6. HSPGs mediate the effect of sulfatase modifying factors on C&E timing. (A) Representative images of 24 hpf zebrafish embryos treated at dome stage (4.33 hpf) with 200 mM or 50 mM of sodium chlorate. **(B)** Representative images of WISH for *tbxta* (mesoderm), *dlx3b* (neural border) and *egr2b* (rhombomeres 3 & 5) in tailbud stage (10 hpf) control and sodium chlorate treated embryos shown from lateral (top) and dorsal (bottom) views. Scale bar 100 µm. **(C, D)** AP axis length (C) and Notochord width (D) (as in Figure 2) of embryos depicted in (B). Each dot represents a single embryo. Means and standard deviation are indicated. **** p<0.0001 compared with WT control embryos by Kruskal–Wallis and Dunn's multiple comparisons tests. **(E)** Onset of extension in *acvr1b** explants of the indicated conditions. Dotted line shows typical extension onset of WT control explants around 8 hpf. Each dot represents a single explant. Means and standard deviation are indicated. N: number of independent experiments, n: number of embryos. ****/ †††† p<0.0001 compared with WT and MZ*sumf1*-/- control groups, respectively, by Kruskal–Wallis and Dunn's multiple comparisons tests. **(F)** Diagram of extracellular heparan sulfate (HS) or water (control) injections in 256-cell embryos prior to explantation (modified from (*36*)). **(G)** Explant extension onset as in (E). ** p>0.01; ****/ ####/ †††† p<0.0001 compared with WT, WT + water, and MZ*sumf2*-/- + water groups, respectively, by Kruskal–Wallis and Dunn's multiple comparisons tests.

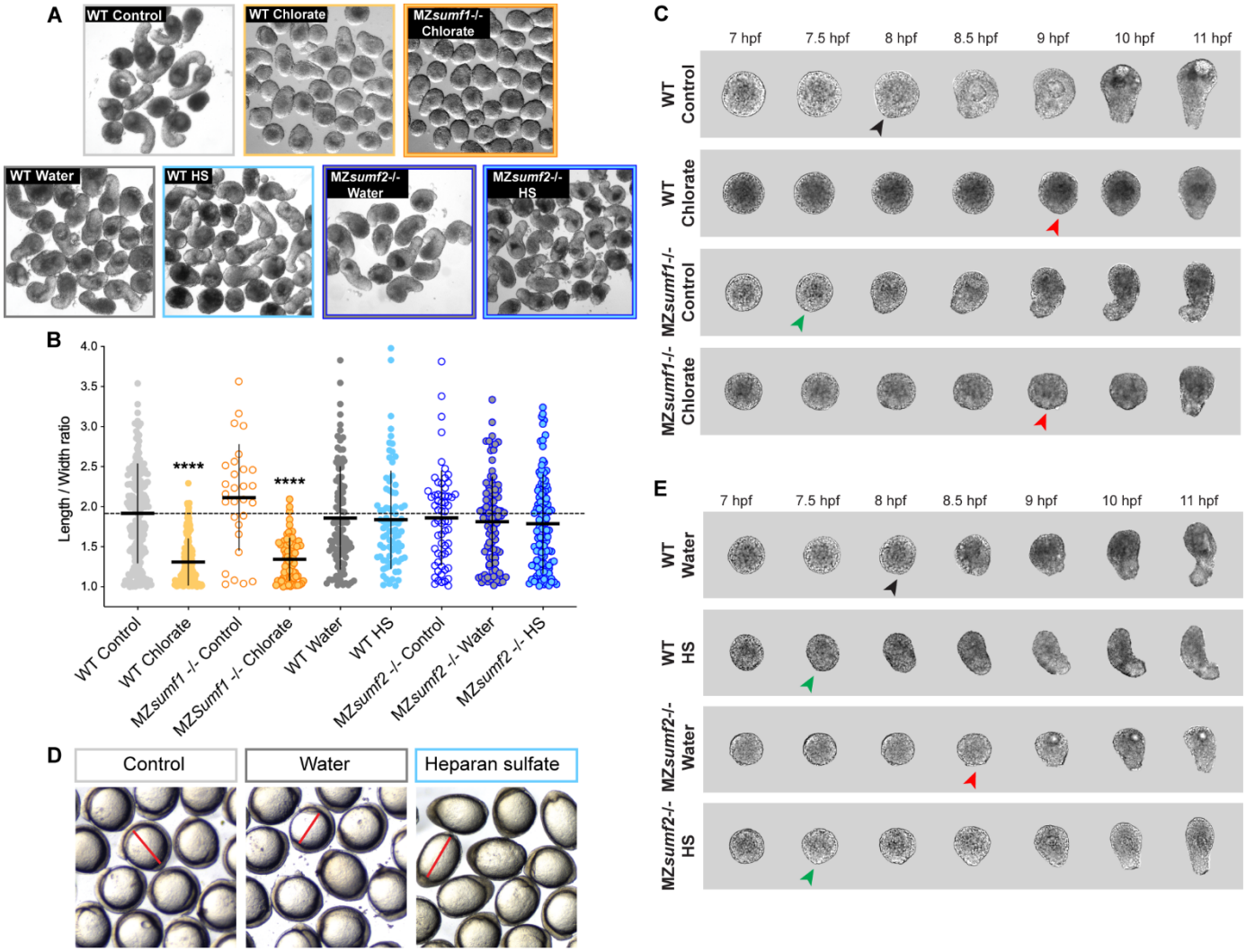

Supplementary Fig. 5. Inhibition of sulfation, but not increased heparan sulfate levels, impairs C&E *ex vivo*. (A) Representative images of *acvr1b** explants from the indicated conditions. **(B)** Length/width ratios of explants shown in (A). Each dot represents a single explant. Means and standard deviation are indicated. **** $p<0.0001$ compared to WT controls by Kruskal–Wallis and Dunn's multiple comparisons tests. **(C)** Representative bright-field images of *acvr1b** explants of the indicated genotypes and treatments over time. Black, red, and green arrowheads indicate timely, precocious, and delayed onset of extension, respectively. **(D)** Heparan sulfate (HS) injected embryos display a dorsalized phenotype at the 2-somite stage (10.66 hpf), indicated by increased animal–vegetal length (red lines). **(E)** Representative bright-field images of *acvr1b** explants of the indicated genotypes and treatments over time, as in (C).

DISCUSSION

Morphogenesis requires precise temporal coordination of cell behaviors to ensure proper tissue shape and function, however, the molecular mechanisms governing its timing remain poorly understood. In this study, we uncover a novel molecular mechanism controlling the timing of C&E morphogenesis. After establishing that transcription is required at gastrulation onset for C&E, we identified the sulfatase modifying factors *sumf1*/FGE and *sumf2*/pFGE as key temporal regulators. Our data support a model (**Fig. 7**) in which, prior to gastrulation, maternally deposited *sumf1*/FGE activates sulfatases enzymes, including the extracellular sulfatase Sulf1. At gastrulation onset, *sumf1* and *sumf2* transcript abundance inverts, and the antagonistic effect of *sumf2*/pFGE on *sumf1*/FGE reduces Sulf1 activity. Consequently, increased levels of sulfated HSPGs promote and/or permit C&E morphogenesis.

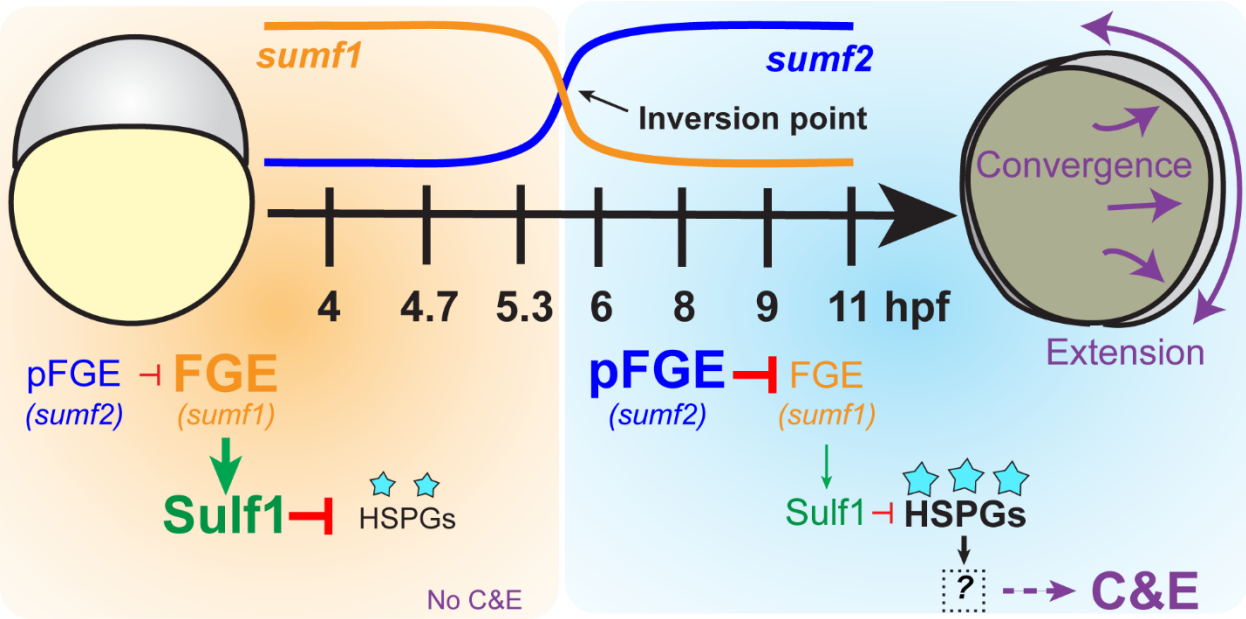

Fig. 7. A model for how sulfatase modifying factors regulate the timing of C&E morphogenesis. Before gastrulation (orange), maternally expressed *sumf1*/FGE activates Sulf1, maintaining low levels of 6-*O*-sulfation (cyan stars) on HSPGs. At the onset of gastrulation (light blue), an inversion in *sumf1* and *sumf2* transcript abundance (inversion point) increases the antagonistic action of *sumf2*/pFGE on *sumf1*/FGE, thereby reducing Sulf1 activity. This shift leads to increased 6-*O*-sulfation of HSPGs, generating a permissive environment for C&E morphogenesis via an unknown downstream mechanism.

478 **Developmental roles of sulfatase modifying factors**

479 This is (to our knowledge) the first report of a role for sulfatase modifying factors in vertebrate
480 gastrulation. In humans, mutations in *SUMF1* cause multiple sulfatase deficiency (MSD), a rare and fatal
481 autosomal recessive disorder characterized by lysosomal dysfunction, developmental delay,
482 neurodegeneration, and skeletal defects including scoliosis, facial dysmorphism, and growth retardation (*55,*
483 *94*). Mouse *Sumf1*-/- models exhibit early postnatal lethality (*95*), and MZ*sumf1*-/- zebrafish recapitulate some
484 MSD features such as cranial malformations and early growth retardation (*78*). However, these fish can survive
485 to adulthood, suggesting the presence of alternative mechanisms of sulfatase activation in this species (*78*).
486 Indeed, *Escherichia coli, Caenorhabditis elegans,* and *Sacchromyces cerevisiae* possess sulfatase genes but
487 lack a Sumf1 homolog, suggesting the existence of an alternative formylglycine generating enzyme in these
488 organisms (*56*). Whether a similar alternative enables MZ*sumf1*-/- zebrafish to survive is unknown.

489 The role of *sumf2*, on the other hand, had not been studied in vertebrate development. Like MZ*sumf1*-/-
490 mutants, we found that MZ*sumf2*-/- fish can reach adulthood and some individuals exhibit scoliosis and
491 craniofacial abnormalities (**Supplementary Fig. 2E**)**.** This indicates that although *sumf2*/pFGE has a significant
492 role in the timing of C&E morphogenesis, it is not ultimately essential for life in zebrafish. Whether its loss is
493 compatible with life in other vertebrate species remains to be tested. Although Sumf1 orthologs are present in
494 prokaryotes, Sumf2 is restricted to eukaryotes and has been lost in several metazoan clades, including
495 arthropods (*55, 75, 94, 96*). *sumf2*/pFGE and *sumf1*/FGE amino acid sequences are highly similar, but
496 *sumf2*/pFGE lacks formylglycine generating activity due to the absence of an active site (*55, 59, 60*). It was
497 shown in human tissue culture that *sumf2*/pFGE reduces *sumf1*/FGE enzymatic activity (*60, 65*), which is
498 thought to occur through direct physical binding and possible interactions with sulfatase enzymes (*59, 65*). This
499 antagonism is consistent with our findings in zebrafish that MZ*sumf2*-/- phenotypes are exacerbated by *sumf1*
500 OE (**Fig. 2**) and co-overexpression of both factors offsets the effects of their individual overexpression (**Fig. 3**).
501 Further, MZ*sumf1*-/-; MZ*sumf2*-/- double mutant explants phenocopy the C&E delay observed in MZ*sumf1*-/-,
502 indicating that *sumf1* is epistatic to *sumf2* (**Fig. 3**), consistent with a model in which *sumf2*/pFGE governs
503 gastrulation cell movements in its capacity as a *sumf1*/FGE inhibitor.

504

505

506 **Sulf1 and HSPGs regulate gastrulation cell movements**

507 Our data implicate Sulf1 as the primary sulfatase affecting C&E timing downstream of *sumf1*/FGE and
508 *sumf2*/pFGE regulation. Sulf1 catalyzes the removal of 6-*O*-sulfation from the D0S6 and D2S6 disaccharides
509 of HSPGs (*67*), precisely the modifications that were increased between early and late zebrafish gastrulation
510 (**Fig. 5**). Notably, this function is also served by the extracellular sulfatases Sulf2a and Sulf2b. However, *sulf2b*
511 OE did not cause pronounced gastrulation phenotypes, and although *sulf2a* OE induced C&E defects in both
512 embryos and explants (**Supplementary Fig. 4**), it did not (unlike *sulf1* OE) alter the onset of explant extension.
513 Although these sulfatases target the same substrate, evidence indicates that human Sulf1 and Sulf2 act on
514 distinct polysaccharide substrates (*97*), which may also explain the differential effects of *sulf1* and *sulf2a/b* in
515 zebrafish gastrulae. While the contribution of other sulfatases cannot be excluded, our finding that *sumf1*
516 overexpression no longer affects C&E onset in the absence of *sulf1* strongly implicates Sulf1 as the key
517 regulator of C&E timing. It is less clear that reduced Sulf1 activity is predominantly responsible for the overall
518 increase in HS levels in later gastrulation, as the abundance and sulfation patterns of HS chains are ultimately
519 determined by the activity of multiple enzymes, including glycosyltransferases, heparinases, sulfatases and
520 sulfotransferases (*98*). Interestingly, *xylosyltransferase I* (*xylt1*), whose activity initiates HS biosynthesis *(97),*
521 was also among our candidate 'trigger' genes upregulated at gastrulation onset (**Fig. 1**), making it an
522 especially compelling candidate for further investigation.

523 HSPGs and the sulfatases that modify them have long been known to regulate gastrulation
524 morphogenesis. For example, elimination of HS chains or loss of HSPG core proteins glypicans and
525 syndecans caused gastrulation defects and/or shortened axes in *Xenopus*, zebrafish, and sea urchin gastrulae
526 (*84, 89, 90, 99-103*). Although our study does not address the HSPG core protein(s) responsible for the
527 observed effects on C&E timing, glypicans and syndecans with established roles in C&E (like *gpc4/kny (101)*)
528 are good candidates. Notably, our manipulations affecting HSPG sulfation tended to produce milder
529 phenotypes that loss of core proteins like Gpc4, consistent with sulfation as a modifier of their activity. Indeed,
530 manipulations that decrease sulfation levels – including overexpression of *sulf1* or *sumf1* mRNA and injection
531 of purified sulfatases into the blastocoel - also disrupted gastrulation in *Xenopus* and sea urchin (*64, 80-82*).
532 Interestingly, loss of sulfatases also caused gastrulation defects (*82, 104, 105*), suggesting that a correct
533 balance of sulfatase activity is required for proper C&E. Our data provide a possible explanation for this:

534 altered timing of C&E movements. We found that *sulf1* overexpression both disrupts and delays C&E, but also
535 that both precocious and delayed C&E onset ultimately cause C&E defects (i.e. shorter and wider embryonic
536 axes) in intact embryos. This raises the possibility that previously reported C&E defects upon gain or
537 (especially) loss of sulfatase function could be the result of altered timing (discussed further below).
538 *sulf1* deficiency, however, not only alters the timing of C&E but also prevents full explant extension (**Fig.
539 4, Supplementary Fig. 4**). This discrepancy in phenotypic severity between Sulf1 and its key regulator
540 (*sumf1*/FGE) may reflect partially independent regulation of sulfatases during zebrafish gastrulation. As
541 discussed above, C&E defects resulting from altered sulfatase activity are relatively mild in zebrafish, and the
542 mutant embryos examined here can ultimately survive to become fertile adults. This suggests the existence of
543 compensatory mechanisms that support continued primary body axis elongation after gastrulation is complete.
544

545 **Temporal dynamics of gastrulation cell movements**

546 Although it is intuitive that delayed C&E ultimately manifests as a C&E defect *in vivo*, it is less clear how
547 increased and/or precocious convergence movements (as seen in MZ*sulf1*-/-, MZ*sumf1*-/-, and *sumf2* OE
548 embryos) lead to similar phenotypes (**Fig. 3 and Fig. 4**). We speculate that all gastrulation cell movements –
549 epiboly, internalization, and C&E – must be coordinated in both space and time to properly shape the nascent
550 body axes. If C&E movements are accelerated, they become out of sync with other concurrent cell
551 movements, disrupting axis extension. This would explain why morphological C&E defects are detected in
552 MZ*sumf1*-/- mutants but not explants (**Fig. 2 and Supplementary Fig. 3**), in which C&E occur in the absence
553 of epiboly and internalization. A similar phenomenon was reported in *Drosophila* gastrulae, in which both
554 slowed and accelerated germ band extension desynchronized morphogenesis between the three germ layers
555 (*106, 107*).
556 It is not yet clear whether sulfatase activity alters the onset of cell movements, their pace, or both. For
557 example, either accelerated cell movements or their precocious onset could manifest as “early onset” of
558 morphological extension within our explants. Indeed, *Drosophila* embryos with loss- and gain-of function
559 mutations in Serotonin signaling components reportedly exhibit slowed and accelerated cell movements driving
560 germ band extension, respectively, without a change in their time of onset (*106-108*). However, our *in vivo* cell-
561 tracking analysis revealed apparent changes in both the onset and speed of convergence movements in

562 zebrafish gastrulae with altered *sumf1, sumf2*, and *sulf1* levels, suggesting that multiple aspects of 'timing' are
563 affected (**Fig. 3 and Fig. 4**). The precise changes in the timing of cell behaviors upon altered sulfatase activity,
564 and their contributions to our observed phenotypes, are areas of interest for future study.
565
566 **How do HSPGs govern morphogenetic timing?**
567 Cell surface and extracellular HSPGs play key roles in multiple morphogen signaling pathways. For
568 example, HSPGs modulate ligand diffusion and availability (*67, 81, 109, 110*) and receptor binding (*67, 81,*
569 *111*) of morphogens with known roles in C&E, including FGF, Wnt, BMP, and Nodal. HSPGs also regulate PCP
570 signaling through binding of non-canonical Wnt ligands (*99, 101, 111*) and membrane localization of
571 Dishevelled (*81, 99, 100*), which is required for PCP activity (*112, 113*). The structural features of HS chains,
572 particularly their sulfation patterns, are critical for these functions as they determine ligand-binding affinity and
573 selectivity (*98, 114, 115*). Notably, the precise role of HSPG sulfation in signaling is context-dependent and
574 changes throughout development. For example, reduced sulfation inhibits and enhances signaling by Wnt8
575 and Wnt11, respectively (*81, 82, 116, 117*), and HSPGs from different developmental stages have different
576 capacities to bind FGF ligands (*118, 119*). We speculate that sulfatase modifiers may regulate C&E timing by
577 controlling HS sulfation, thereby modulating the degree and dynamics of HSPG-mediated signaling. Indeed,
578 we observed an increase in the levels of sulfated HSPGs (Sulf1 substrates) during late gastrulation (**Fig. 5**)
579 and demonstrated that both decreased and increased levels of sulfated HS were sufficient to alter C&E timing
580 (**Fig. 6**). Importantly, the phenotypes associated with *sumf1/2* and *sulf1* perturbations reflect disrupted
581 morphogenesis in the absence of obviously altered cell fate specification, as embryos still give rise to
582 derivatives of all three germ layers, consistent with observations in *Xenopus* and sea urchin gastrulation (*80,*
583 *84*). However, we cannot exclude the possibility that the alterations in C&E timing are secondary to subtle
584 patterning defects or changes in the timing of cell fate choices. Whether this putative role in morphogen
585 signaling underlies the effect of sulfatase modifiers on C&E timing will be an exciting topic for future studies.
586
587
588

589 **METHODS**

590

591 **Zebrafish**

592 Adult zebrafish were maintained following established protocols (*120*) in compliance with Baylor College of
593 Medicine Institutional Animal Care and Use Committees. Embryos were obtained through natural mating, and
594 staging was based on established morphology (*121*). Fish were chosen from their home tank to be crossed at
595 random, and embryos were randomly chosen from the clutch for injection and inclusion in experiments. WT
596 and mutant embryos were collected in parallel in a period not longer than 10–15 min to minimize
597 developmental differences and raised in egg water at 28.5°C under identical conditions. Experiments on WT
598 embryos were conducted in either the AB or TU background, depending on the background of the mutant line
599 used. The mutant lines used were *sum*^{la015919Tg} (ZFIN ID: ZDBALT-120806-11568), *sulf1*^{sjr9} (Kaur et al,
600 submitted), *sumf2*^{bcm126} (this study, described further below) and *oep*^{tz257} *(101). oep-/-* embryos were rescued to
601 viability by injection of 50 pg of *oep* mRNA *(122)* and raised to adulthood, then intercrossed to generate
602 MZ*oep-/-* embryos for explantation. MZ*sumf1*-/-; MZ*sumf2*-/- double mutants were generated by crossing
603 single homozygous mutants to obtain double heterozygotes, which were subsequently incrossed.

604

605 ***sumf2*^{bcm126} generation and genotyping**

606 *sumf2* zebrafish mutants were generated using the CRISPR–Cas9 system. A single guide (sg)RNA targeting
607 exon 2 of *sumf2* (5′-GGATGGAGAATCGCCAACAC-3′) was designed using CRISPRscan (*123*). sgRNAs were
608 transcribed using T7 RNA polymerase (NEB, M0251S) from DNA templates generated with the forward primer
609 (Fw): gaaattaatacgactcactataGGATGGAGAATCGCCAACACgttttagagctagaaatagc, and the reverse primer
610 (Rv): aaaagcaccgactcggtgccactttttcaagttgataacggactagccttattttaacttgctatttctagctctaaaac. 1 µl of gRNA was pre-
611 incubated for 10 min at 37 °C with Cas9 protein (NEB, M0646M) and 300mM KCl (as described by (*124*)). AB
612 WT Embryos were injected at the single-cell stage with 1 nl of the gRNA–Cas9 complex and cutting efficiency
613 was assessed using a T7 endonuclease I assay (*125*). A PCR fragment encompassing the target sequence
614 was amplified from genomic DNA (gDNA) of individual embryos (using the following primers: Fw:
615 AGATGGTGTTTATTCCTGGTGG, Rv: TCCTCTGATACAAAATCCTGGAA) and incubated with T7
616 endonuclease I (NEB #M0302L) in NEB 10× Buffer 2. Injected F0 embryos were raised and outcrossed to AB

617 WT fish. F1 progeny were genotyped by Sanger sequencing to identify transmitted mutations. A 7 bp insertion
618 in exon 2 of *sumf2* (sumf2^{bcm126}), resulting in an early stop codon, was selected (**Supplementary Fig. 2A**). This
619 mutation introduced an XcmI restriction site, enabling genotyping by digestion of the PCR-amplified target
620 fragment with XcmI (NEB, R0533S) (**Supplementary Fig. 2B**). Heterozygous F1 carriers were incrossed to
621 produce the F2 generation. Homozygotes F2 fish were raised and incrossed to obtained MZ*sumf2*-/- embryos
622 for experiments.
623

624 **RT-qPCR**

625 RNA was isolated from 50 pooled WT and MZ*sumf2*-/- 24 hpf larvae from three independent clutches. Total
626 RNA was extracted using TRIzol reagent (Thermo Fisher Scientific, 15596018), purified by sodium acetate
627 precipitation, eluted in 10 mM Tris pH7.5 and treated with Turbo DNAase I (Invitrogen, AM2238) at 37°C for 30
628 min. For each sample, 1μg of the RNA was reverse-transcribed using iScript Reverse Transcription Supermix
629 for RT-qPCR (Biorad, #1708840). *sumf2* specific primers were designed to span exon-exon junctions [Exon 1-
630 2 (pair 1) FW: CACAGTGTCTTGTGCAGCAG, RV: AGTTGGAGTTGGTGACAGGA; Exon 3-5 (pair 2) FW:
631 GGCTGAAACATTTGGCTGGA, RV: GGCATCATTCCAGCTGACCT]. *rpl13a-1* was used as a housekeeping
632 gene [FW: TCTGGAGGACTGTAAGAGGTATGC, RV: AGACGCACAATCTTGAGAGCAG]. qPCR was
633 performed in technical triplicates using SsoAdvanced Universal SYBR Green Supermix (Biorad, #1725270).
634 Relative expression levels were calculated using the $2^{-\Delta\Delta Ct}$ method.
635

636 **Preparation and microinjection of mRNA**

637 All mRNAs were transcribed using the SP6 mMessage mMachine Kit (Fisher Scientific, AM1340) and purified
638 using Bio -Rad Microbiospin columns (Bio-Rad, 7326250). Single-celled embryos were placed in agarose
639 molds (Adaptive Science Tools, I-34) and injected with 0.5-1 nl volumes using pulled glass needles (Fisher
640 Scientific, 50-821-984). Doses of mRNA per embryo were as follows: 0.5 pg *acvr1b** (*69*), 10 pg *ndr2* (*126*),
641 50-100 pg s*umf1*, 100 pg *sumf2*, 500 pg *sfGFP,* 500 pg *sulf2b,* 500 pg *sulf2a,* 500pg *gnsb,* 50-500 pg *sulf1,*
642 500 pg *sgsh,* 500 pg *arsb,* 500 pg *gnsa,* 500 pg *ids,* 500 pg *galns,* 500 pg *arsa,* 500 pg *sts,* 100 pg *mem-GFP*
643 and 100 pg *H2B-scarlet.* Templates for *sumf1*, *sumf2*, and all sulfatases were generated by Gibson cloning

644 (*127*) each of their open reading frames (synthesized by Twist Biosciences) into a PJS2 vector linearized with
645 EcoRI.
646
647 **Whole mount *in situ* hybridization (WISH)**
648 *tbxta (brachyury, t)*, *dlx3b* and *egr2b (krox20)* antisense riboprobes were transcribed using NEB T7 RNA
649 polymerase (NEB, M0251s) and labeled with digoxigenin NTPs (Sigma/Millipore, 11277073910) NTPs
650 (Sigma/Millipore, 11685619910). WISH was performed according to (*128*). Embryos were fixed overnight in at
651 4°C 4% PFA in PBS, rinsed in PBS + 10% tween-20 (PBT), and dehydrated into methanol. Following
652 rehydration into PBT, embryos were pre-incubated for at least two hours in hybridization buffer with 50%
653 formamide (in 0.75 M sodium chloride, 75 mM sodium citrate, 0.1% tween 20, 50 mg/mL heparin (Sigma), and
654 200 mg/mL tRNA) at 70°C, and hybridized overnight at 70°C with antisense probes (1-5 ng/mL) in hybridization
655 buffer. Samples were washed gradually into 2X SSC buffer (0.3 M sodium chloride, 30 mM sodium citrate),
656 and then gradually from SSC to PBT. Samples were blocked at room temperature for several hours in PBT
657 with 2% goat serum and 2 mg/mL bovine serum albumin (BSA), then incubated overnight at 4°C with anti-DIG
658 antibody (Roche #11093274910) at 1:5000 in block. After extensive washes in PBT, embryos were rinsed in
659 staining buffer (PBT +100 mM Tris pH 9.5, 50 mM $MgCl_2$, and 100 mM NaCl) and developed in BM Purple AP
660 substrate (Roche) until the desired staining intensity was achieved. Staining was stopped with 10 mM EDTA in
661 PBT before imaging.
662
663 **Blastoderm explants**
664 Blastoderm explants were prepared as described by (*129*). Briefly, uninjected, *acvr1b*-,* or *ndr2*-injected
665 embryos were dechorionated at the 256-cell stage using pronase (Roche; 1 ml of 20 mg/ml stock in 15 ml 3×
666 Danieau's solution). At the 512-cell stage, approximately 1/3 of the most animal blastoderm cells were excised
667 using Dumont #55 forceps (Fisher Scientific, NC9791564) on an agarose-coated plate containing 3× Danieau's
668 solution. Explants were allowed to heal briefly before being transferred into agarose-coated 6-well plates
669 containing explant medium [Dulbecco's modified eagle medium with nutrient mixture F-12 (Gibco 11330032)
670 containing 2.5 mM L-glutamine, 15 mM HEPES, 3% newborn calf serum (Invitrogen 26010–066), 50 units/mL
671 penicillin, and 50 mg/mL streptomycin (10,000 U/mL pen-strep at 1:200, Gibco 15140163)]. Explants were

incubated at 28.5 °C until sibling embryos from the same genetic background reached the desired developmental stage.

Alcian Blue staining

Embryos were fixed in PFA 4% overnight, extensively washed in PBS, and incubated in Alcian Blue staining solution pH 1 (0.2% Alcian Blue 8 GX (Sigma # A5268), 50% ethanol, ~0.1N HCl) for 48 h at room temperature, protected from light. Samples were then gradually rehydrated into PBS, post-fixed in 4% PFA, washed with PBS, and rinsed in 2% KOH. Embryos were cleared through a graded series of glycerol in 2% KOH (20%, 40%, 60%) and stored in 80% glycerol in 2% KOH for imaging and long-term storage.

Transcription inhibitor treatment

1 μM Triptolide (Sigma # T3652) or an equivalent volume of DMSO was added to the media of blastoderm explants in agarose-coated 6-well plates at 50% (4.7 hpf), shield (6 hpf), 70% (7.5 hpf) or 80% (8.5 hpf). 0.5 μM Flavopiridol (Selleck, S1230) or an equivalent volume of DMSO was added to the media of blastoderm explants at 50% (4.7 hpf) and washed-out twice with 0.3x Danieau solution, before incubation with fresh explant medium.

Sodium Chlorate treatment

Dome stage (4.33 hpf) embryos or blastoderm explants were treated with 200 or 50 mM of Sodium Chlorate (VWR # 7775-09-9) in egg water or explant medium.

Heparan Sulfate injections

Uninjected or *acvr1b**-injected embryos were dechorionated at the 64-cell stage using pronase (Roche; 1 mL of 20 mg/mL stock in 15 mL 3× Danieau's solution). Embryos were transferred to agarose-coated plates containing cubical depressions (Adaptive Science Tools, PT-1) filled with 0.3× Danieau's solution. At the 256-cell stage, embryos were injected with 2 nL of 5 ng/mL heparan sulfate (Sigma-Aldrich, H7640) or nuclease-free water into the extracellular space.

700 **Microscopy**

701 Live embryos injected with *H2B-mScarlet* and *mem-GFP* mRNA were manually dechorionated and mounted in
702 0.3-0.35% low-melt agarose (Thermo Fisher Scientific, 16520100) in glass-bottomed 35 mm Petri dishes
703 (Fisher Scientific, FB0875711YZ) for imaging using a Nikon ECLIPSE Ti2 inverted confocal microscope
704 equipped with a Yokogawa W1 spinning disk unit, PFS4 camera, and 405/488/561 nm lasers (emission filters:
705 455/50, 525/36, 605/52). Temperature was maintained at 28.5°C during imaging using a Tokai Hit STX stage
706 top Incubator. For live time-lapse series, 100 µm z-stacks with a 2 µm step were collected every 5 minutes for
707 5 hours using a Plan Apo Lambda 20x dry objective lens. Live blastoderm explants were mounted in rounded
708 chambers made in 1% low-melt agarose in glass-bottomed dishes containing explants medium and imaged in
709 the same scope. For live time-lapses, 14 µm z-stacks were obtained with a 2 µm step every 10 minutes for 6
710 hours using a Plan Apo Lambda 10x dry objective lens. Images of WISH and alcian blue-stained embryos and
711 live embryos, larvae and explants were taken with a Nikon Fi3 color camera on a Nikon SMZ745T
712 stereoscope.

713

714 **Image analysis**

715 ImageJ/Fiji was used to visualize and measure all microscopy data sets.

716

717 *Morphometric analyses*

718 During analysis, researchers were kept unaware of the conditions of all image data using the blind_renamer
719 Perl script (https://github.com/jimsalterjrs/blindanalysis) (blindanalysis: v.1.0.) prior to analysis. To measure the
720 length/width ratios of explants, the length of a segmented line drawn along the midline of each explant
721 (accounting for curvature) was divided by the length of a perpendicular line spanning the maximal width of the
722 explant. Tailbud morphometries were performed in whole-mount embryos staged using *egr2b* expression at the
723 future mid-hindbrain boundary. Notochord width was quantified in dorsal-view images as the mediolateral
724 extent of the *tbxta* expression domain at the midline. Anteroposterior (AP) axis length was measured in lateral-
725 view images from the anterior to posterior boundaries of the *dlx3b* expression domain.

726

727

728 *Explant onset of extension*

729 The onset of explant extension was assessed in a blinded manner as the time point when a visible tip first
730 emerged from an initially rounded explant. Explant were staged according to sibling intact embryos from the
731 same genetic background cultured in the same plate.

732

733 *Cell tracking analysis*

734 Automated nuclear tracking was performed using the ImageJ TrackMate7 plugin (*130*) in the dorsal
735 hemisphere (encompassing dorsal and lateral cells) of zebrafish gastrulae injected with *H2B-scarlet* mRNA.
736 TrackMate generated color-coded trajectories and measurements of mediolateral (ML) displacement. Embryos
737 were staged relative to formation of the second somite. To minimize noise from reduced convergence
738 movements near the dorsal midline, cells within 100 µm of the midline were excluded from the analysis.
739 Average displacement in the X (ML) dimension was calculated per time frame, smoothed using a sliding
740 window of four time points, and plotted over time using GraphPad Prism 10.

741

742 **GAG isolation and disaccharide analysis.**

743 Whole zebrafish gastrulae (5.3 or 8.5 hpf, 100 embryos/sample) were homogenized and lysed in 0.5% CHAPS
744 lysis buffer (50 mM HEPES, 120 mM NaCl, 2 mM EDTA, pH 7.4) containing a protease inhibitor cocktail (Roche).
745 50 µL of cell lysate was set aside for protein quantification via BCA assay. Homogenates were diluted 1:10 in a
746 wash buffer (50 mM sodium acetate, 200 mM NaCl, 0.1% Triton X-100, pH 6.0) and incubated with Pronase (0.4
747 mg/ml, Sigma) overnight at 37 °C with mild agitation. The product was centrifuged (4,000 xg, 20 minutes) then
748 passed through a DEAE-Sephacel (Cytiva) column equilibrated in 50 mM sodium acetate buffer, pH 6.0,
749 containing 200 mM NaCl, and desalted using a PD-10 desalting column (Cytiva). The purified GAGs were
750 subsequently enzymatically depolymerized with 2 mU each of heparin lyases I-III (IBEX) and differentially mass
751 labeled by reductive amination with aniline, as described (*87*). Tagged HS disaccharides were analyzed by HILIC-
752 Q-TOF-MS on a Waters Synapt XS Q-TOF mass spectrometer, as previously described (*87*). Samples were
753 quantified using isotopically labeled internal disaccharide standards and normalized to total protein, as measured
754 by BCA.

755

756 **Statistical analysis**

757 Number of embryos (n) and independent experimental replicates (N) for animal studies are stated in graphs. All
758 experiments were performed at least in triplicates. GraphPad Prism 10 software was used to perform statistical
759 analyses and generate graphs for all data analyzed. Datasets were tested for normality prior to analysis and
760 statistical tests were chosen accordingly. The statistical tests used for each data set are noted in figure
761 legends.

762

763 **ACKNOWLEDGEMENTS**

764 We thank Dr. Lila Solnica-Krezel for sharing plasmids and WISH probes, the BCM Center for Comparative
765 Medicine for taking excellent care of our fish, and the Zebrafish International Resource Center for preserving
766 and distributing fish lines used here and by countless members of the community. Thanks also to all members
767 of the Williams lab for their help and feedback on this project, and Drs. Maria Cecilia Cirio and Lance Davidson
768 for their thoughtful comments on the manuscript.

769

770 **COMPETING INTERESTS**

771 The authors declare no competing interests.

772

773 **AUTHOR CONTRIBUTIONS**

774 A.S.C. and M.K.W. conceived of the project. A.S.C. and M.K.W. performed zebrafish experiments, R.J.W. and
775 A.B. performed HS disaccharide profiling, and R.M.J. and G.K.B. generated the *sulf1* deletion line. S.G. and
776 C.C. performed bioinformatic analysis. A.S.C and M.K.W. wrote the original manuscript. All authors reviewed
777 the manuscript.

778

779 **FUNDING**

780 This work was supported by NIH/NICHD grants R00HD091386 and R01HD104784 to M.K.W. R.J.W. is
781 supported by NIH grant R35GM150736. The glycosaminoglycan disaccharide analyses performed at the
782 CCRC were partially supported by NIH grant R24GM137782 to Parastoo Azadi. G.K.B. was supported by a
783 Bourses d'excellence (Université de Montréal) and a FRQ Doctoral Scholarship. R.M.J. is supported by CIHR

grants (PJT-178037, PJT-204048) and FRQS J1 and J2 awards. S.G. and C.C. were partially supported by CPRIT RP210227 and RP200504, NIH/NCI P30 shared resource grant CA125123, NIH/NIEHS P42 ES027725 and P30 ES030285. Data analysis was performed on the HPC cluster that is managed by the Biostatistics and Informatics Shared Resource (BISR) and supported by an NIH S10 Shared Instrument Grant S10-OD032185, NCI P30-CA125123 and Institutional funds from the Dan L Duncan Comprehensive Cancer Center and Baylor College of Medicine.

REFERENCES

1. K. K. Smith, Time's arrow: heterochrony and the evolution of development. *Int J Dev Biol* **47**, 613-621 (2003).
2. K. K. Smith, Sequence heterochrony and the evolution of development. *J Morphol* **252**, 82-97 (2002).
3. N. I. Petridou, S. Grigolon, G. Salbreux, E. Hannezo, C. P. Heisenberg, Fluidization-mediated tissue spreading by mitotic cell rounding and non-canonical Wnt signalling. *Nat Cell Biol* **21**, 169-178 (2019).
4. N. I. Petridou, B. Corominas-Murtra, C. P. Heisenberg, E. Hannezo, Rigidity percolation uncovers a structural basis for embryonic tissue phase transitions. *Cell* **184**, 1914-1928.e1919 (2021).
5. E. G. Hagos, S. T. Dougan, Time-dependent patterning of the mesoderm and endoderm by Nodal signals in zebrafish. *BMC Dev Biol* **7**, 22 (2007).
6. *D. Pinheiro*, *R.* K*ardos*, *É. H.* H*annezo, Carl-Philipp*, *Morphogen gradient orchestrates pattern-preserving tissue morphogenesisvia motility-driven unjamming*. *Nature Physics* **18**, *1482–1493* (2022).
7. Z. Liu, S. Woo, O. D. Weiner, Nodal signaling has dual roles in fate specification and directed migration during germ layer segregation in zebrafish. *Development* **145**, (2018).
8. Y. Moriyama, T. Mitsui, C. P. Heisenberg, Hoxb genes determine the timing of cell ingression by regulating cell surface fluctuations during zebrafish gastrulation. *Development* **152**, (2025).
9. T. Iimura, O. Pourquié, Collinear activation of Hoxb genes during gastrulation is linked to mesoderm cell ingression. *Nature* **442**, 568-571 (2006).
10. J. B. Wallingford, R. M. Harland, Xenopus Dishevelled signaling regulates both neural and mesodermal convergent extension: parallel forces elongating the body axis. *Development* **128**, 2581-2592 (2001).
11. J. B. Wallingford, R. M. Harland, Neural tube closure requires Dishevelled-dependent convergent extension of the midline. *Development* **129**, 5815-5825 (2002).
12. L. A. Davidson, R. E. Keller, Neural tube closure in Xenopus laevis involves medial migration, directed protrusive activity, cell intercalation and convergent extension. *Development* **126**, 4547-4556 (1999).
13. R. Keller, L. A. Davidson, D. R. Shook, How we are shaped: the biomechanics of gastrulation. *Differentiation* **71**, 171-205 (2003).
14. R. Keller *et al.*, Mechanisms of convergence and extension by cell intercalation. *Philos Trans R Soc Lond B Biol Sci* **355**, 897-922 (2000).
15. R. J. Huebner, J. B. Wallingford, Coming to Consensus: A Unifying Model Emerges for Convergent Extension. *Dev Cell* **46**, 389-396 (2018).
16. J. Shih, R. Keller, Cell motility driving mediolateral intercalation in explants of Xenopus laevis. *Development* **116**, 901-914 (1992).
17. J. Shih, R. Keller, Patterns of cell motility in the organizer and dorsal mesoderm of Xenopus laevis. *Development* **116**, 915-930 (1992).
18. M. L. Concha, R. J. Adams, Oriented cell divisions and cellular morphogenesis in the zebrafish gastrula and neurula: a time-lapse analysis. *Development* **125**, 983-994 (1998).
19. D. S. Sepich, C. Calmelet, M. Kiskowski, L. Solnica-Krezel, Initiation of convergence and extension movements of lateral mesoderm during zebrafish gastrulation. *Dev Dyn* **234**, 279-292 (2005).
20. B. Schmid *et al.*, High-speed panoramic light-sheet microscopy reveals global endodermal cell dynamics. *Nat Commun* **4**, 2207 (2013).

21. D. C. Myers, D. S. Sepich, L. Solnica-Krezel, Bmp activity gradient regulates convergent extension during zebrafish gastrulation. *Dev Biol* **243**, 81-98 (2002).
22. H. Ninomiya, R. P. Elinson, R. Winklbauer, Antero-posterior tissue polarity links mesoderm convergent extension to axial patterning. *Nature* **430**, 364-367 (2004).
23. R. Keller, J. Shih, A. K. Sater, C. Moreno, Planar induction of convergence and extension of the neural plate by the organizer of Xenopus. *Dev Dyn* **193**, 218-234 (1992).
24. R. S. Gray, I. Roszko, L. Solnica-Krezel, Planar cell polarity: coordinating morphogenetic cell behaviors with embryonic polarity. *Dev Cell* **21**, 120-133 (2011).
25. J. B. Wallingford, S. E. Fraser, R. M. Harland, Convergent extension: the molecular control of polarized cell movement during embryonic development. *Dev Cell* **2**, 695-706 (2002).
26. R. Bastock, H. Strutt, D. Strutt, Strabismus is asymmetrically localised and binds to Prickle and Dishevelled during Drosophila planar polarity patterning. *Development* **130**, 3007-3014 (2003).
27. C. Yin, M. Kiskowski, P. A. Pouille, E. Farge, L. Solnica-Krezel, Cooperation of polarized cell intercalations drives convergence and extension of presomitic mesoderm during zebrafish gastrulation. *J Cell Biol* **180**, 221-232 (2008).
28. B. Ciruna, A. Jenny, D. Lee, M. Mlodzik, A. F. Schier, Planar cell polarity signalling couples cell division and morphogenesis during neurulation. *Nature* **439**, 220-224 (2006).
29. M. T. Butler, J. B. Wallingford, Spatial and temporal analysis of PCP protein dynamics during neural tube closure. *Elife* **7**, (2018).
30. I. Roszko, D. S Sepich, J. R. Jessen, A. Chandrasekhar, L. Solnica-Krezel, A dynamic intracellular distribution of Vangl2 accompanies cell polarization during zebrafish gastrulation. *Development* **142**, 2508-2520 (2015).
31. S. von der Hardt *et al.*, The Bmp gradient of the zebrafish gastrula guides migrating lateral cells by regulating cell-cell adhesion. *Curr Biol* **17**, 475-487 (2007).
32. M. Constance Lane, L. Davidson, M. D. Sheets, BMP antagonism by Spemann's organizer regulates rostral–caudal fate of mesoderm. *Developmental Biology* **275**, 356-374 (2004).
33. W. Shi, S. M. Peyrot, E. Munro, M. Levine, FGF3 in the floor plate directs notochord convergent extension in the Ciona tadpole. *Development* **136**, 23-28 (2009).
34. E. Aamar, D. Frank, Xenopus Meis3 protein forms a hindbrain-inducing center by activating FGF/MAP kinase and PCP pathways. *Development* **131**, 153-163 (2004).
35. B. Gao *et al.*, Coordinated directional outgrowth and pattern formation by integration of Wnt5a and Fgf signaling in planar cell polarity. *Development* **145**, (2018).
36. M. L. K. Williams, L. Solnica-Krezel, Nodal and Planar Cell Polarity signaling cooperate to regulate zebrafish convergence and extension gastrulation movements. *Elife* **9**, (2020).
37. G. Luxardi, L. Marchal, V. Thomé, L. Kodjabachian, Distinct Xenopus Nodal ligands sequentially induce mesendoderm and control gastrulation movements in parallel to the Wnt/PCP pathway. *Development* **137**, 417-426 (2010).
38. K. Symes, J. C. Smith, Gastrulation movements provide an early marker of mesoderm induction in Xenopus laevis. *Development*, 339-349 (1987).
39. J. Minshull *et al.*, The role of cyclin synthesis, modification and destruction in the control of cell division. *J Cell Sci Suppl* **12**, 77-97 (1989).
40. J. Newport, M. Kirschner, A major developmental transition in early Xenopus embryos: I. characterization and timing of cellular changes at the midblastula stage. *Cell* **30**, 675-686 (1982).
41. H. Chen, L. C. Einstein, S. C. Little, M. C. Good, Spatiotemporal Patterning of Zygotic Genome Activation in a Model Vertebrate Embryo. *Dev Cell* **49**, 852-866.e857 (2019).
42. S. Chari, H. Wilky, J. Govindan, A. A. Amodeo, Histone concentration regulates the cell cycle and transcription in early development. *Development* **146**, (2019).
43. S. R. Joseph *et al.*, Competition between histone and transcription factor binding regulates the onset of transcription in zebrafish embryos. *Elife* **6**, (2017).
44. C. Collart, G. E. Allen, C. R. Bradshaw, J. C. Smith, P. Zegerman, Titration of four replication factors is essential for the Xenopus laevis midblastula transition. *Science* **341**, 893-896 (2013).
45. J. Newport, M. Kirschner, A major developmental transition in early Xenopus embryos: II. Control of the onset of transcription. *Cell* **30**, 687-696 (1982).
46. T. Itoh, A. Shinagawa, Timing system for the start of gastrulation in the Xenopus embryo. *Dev Growth Differ* **45**, 261-273 (2003).

47. S. Kuroda, T. Satoh, A. Shinagawa, Involvement of a urethane-sensitive system in timing the onset of gastrulation in Xenopus laevis embryos. *Dev Growth Differ* **43**, 401-413 (2001).
48. M. Takagi, T. Shimoda, A. Shinagawa, Dependence of the timing system regulating the onset of gastrulation on cytoplasmic, but not nuclear, activities in the Xenopus embryo. *Dev Growth Differ* **47**, 415-422 (2005).
49. K. Hara, P. Tydeman, M. Kirschner, A cytoplasmic clock with the same period as the division cycle in Xenopus eggs. *Proc Natl Acad Sci U S A* **77**, 462-466 (1980).
50. E. V. Chulitskaia, Desynchronization of cell divisions in the course of egg cleavage and an attempt at experimental shift of its onset. *J Embryol Exp Morphol* **23**, 359-374 (1970).
51. Y. Kobayakawa, H. Y. Kubota, Temporal pattern of cleavage and the onset of gastrulation in amphibian embryos developed from eggs with the reduced cytoplasm. *J Embryol Exp Morphol* **62**, 83-94 (1981).
52. I. J. T. Strong, X. Lei, F. Chen, K. Yuan, P. H. O'Farrell, Interphase-arrested Drosophila embryos activate zygotic gene expression and initiate mid-blastula transition events at a low nuclear-cytoplasmic ratio. *PLoS Biol* **18**, e3000891 (2020).
53. M. Almuedo-Castillo *et al.*, Scale-invariant patterning by size-dependent inhibition of Nodal signalling. *Nat Cell Biol* **20**, 1032-1042 (2018).
54. D. A. Kane *et al.*, The zebrafish epiboly mutants. *Development* **123**, 47-55 (1996).
55. T. Dierks *et al.*, Multiple sulfatase deficiency is caused by mutations in the gene encoding the human C(alpha)-formylglycine generating enzyme. *Cell* **113**, 435-444 (2003).
56. J. Landgrebe, T. Dierks, B. Schmidt, K. von Figura, The human SUMF1 gene, required for posttranslational sulfatase modification, defines a new gene family which is conserved from pro- to eukaryotes. *Gene* **316**, 47-56 (2003).
57. J. Peng *et al.*, Eukaryotic formylglycine-generating enzyme catalyses a monooxygenase type of reaction. *FEBS J* **282**, 3262-3274 (2015).
58. A. Preusser-Kunze *et al.*, Molecular characterization of the human Calpha-formylglycine-generating enzyme. *J Biol Chem* **280**, 14900-14910 (2005).
59. A. Dickmanns *et al.*, Crystal structure of human pFGE, the paralog of the Calpha-formylglycine-generating enzyme. *J Biol Chem* **280**, 15180-15187 (2005).
60. M. Mariappan *et al.*, Expression, localization, structural, and functional characterization of pFGE, the paralog of the Calpha-formylglycine-generating enzyme. *J Biol Chem* **280**, 15173-15179 (2005).
61. M. Mariappan *et al.*, The non-catalytic N-terminal extension of formylglycine-generating enzyme is required for its biological activity and retention in the endoplasmic reticulum. *J Biol Chem* **283**, 11556-11564 (2008).
62. T. Dierks *et al.*, Molecular basis for multiple sulfatase deficiency and mechanism for formylglycine generation of the human formylglycine-generating enzyme. *Cell* **121**, 541-552 (2005).
63. D. Roeser *et al.*, A general binding mechanism for all human sulfatases by the formylglycine-generating enzyme. *Proc Natl Acad Sci U S A* **103**, 81-86 (2006).
64. T. Sakuma *et al.*, HpSumf1 is involved in the activation of sulfatases responsible for regulation of skeletogenesis during sea urchin development. *Dev Genes Evol* **221**, 157-166 (2011).
65. E. Zito *et al.*, Sulphatase activities are regulated by the interaction of sulphatase-modifying factor 1 with SUMF2. *EMBO Rep* **6**, 655-660 (2005).
66. K. Uchimura, M. Morimoto-Tomita, S. D. Rosen, Measuring the activities of the Sulfs: two novel heparin/heparan sulfate endosulfatases. *Methods Enzymol* **416**, 243-253 (2006).
67. X. Ai *et al.*, QSulf1 remodels the 6-O sulfation states of cell surface heparan sulfate proteoglycans to promote Wnt signaling. *J Cell Biol* **162**, 341-351 (2003).
68. M. Morimoto-Tomita, K. Uchimura, Z. Werb, S. Hemmerich, S. D. Rosen, Cloning and characterization of two extracellular heparin-degrading endosulfatases in mice and humans. *J Biol Chem* **277**, 49175-49185 (2002).
69. A. Renucci, V. Lemarchandel, F. Rosa, An activated form of type I serine/threonine kinase receptor TARAM-A reveals a specific signalling pathway involved in fish head organiser formation. *Development* **122**, 3735-3743 (1996).
70. D. V. Titov *et al.*, XPB, a subunit of TFIIH, is a target of the natural product triptolide. *Nat Chem Biol* **7**, 182-188 (2011).
71. A. A. Emig *et al.*, Temporal dynamics of BMP/Nodal ratio drive tissue-specific gastrulation morphogenesis. *Development* **152**, (2025).

72. K. Gritsman *et al.*, The EGF-CFC protein one-eyed pinhead is essential for nodal signaling. *Cell* **97**, 121-132 (1999).
73. S. H. Chao, D. H. Price, Flavopiridol inactivates P-TEFb and blocks most RNA polymerase II transcription in vivo. *J Biol Chem* **276**, 31793-31799 (2001).
74. R. J. White *et al.*, A high-resolution mRNA expression time course of embryonic development in zebrafish. *Elife* **6**, (2017).
75. M. P. Cosma *et al.*, Molecular and functional analysis of SUMF1 mutations in multiple sulfatase deficiency. *Hum Mutat* **23**, 576-581 (2004).
76. M. Buono, M. P. Cosma, Sulfatase activities towards the regulation of cell metabolism and signaling in mammals. *Cell Mol Life Sci* **67**, 769-780 (2010).
77. P. Bojarová, S. J. Williams, Sulfotransferases, sulfatases and formylglycine-generating enzymes: a sulfation fascination. *Current Opinion in Chemical Biology* **12**, 573-581 (2008).
78. A. Fleming *et al.*, Unexpected Phenotype Reversion and Survival in a Zebrafish Model of Multiple Sulfatase Deficiency. *Front Cell Dev Biol* **10**, 843079 (2022).
79. N. S. Glickman, C. B. Kimmel, M. A. Jones, R. J. Adams, Shaping the zebrafish notochord. *Development* **130**, 873-887 (2003).
80. J. B. Wallingford, A. K. Sater, J. A. Uzman, M. V. Danilchik, Inhibition of morphogenetic movement during Xenopus gastrulation by injected sulfatase: implications for anteroposterior and dorsoventral axis formation. *Dev Biol* **187**, 224-235 (1997).
81. S. W. Fellgett, R. J. Maguire, M. E. Pownall, Sulf1 has ligand-dependent effects on canonical and non-canonical Wnt signalling. *J Cell Sci* **128**, 1408-1421 (2015).
82. S. D. Freeman *et al.*, Extracellular regulation of developmental cell signaling by XtSulf1. *Dev Biol* **320**, 436-445 (2008).
83. K. Mitsunaga-Nakatsubo, Y. Akimoto, H. Kawakami, K. Akasaka, Sea urchin arylsulfatase, an extracellular matrix component, is involved in gastrulation during embryogenesis. *Dev Genes Evol* **219**, 281-288 (2009).
84. K. F. Bergeron, X. Xu, B. P. Brandhorst, Oral-aboral patterning and gastrulation of sea urchin embryos depend on sulfated glycosaminoglycans. *Mech Dev* **128**, 71-89 (2011).
85. P. A. Baeuerle, W. B. Huttner, Chlorate--a potent inhibitor of protein sulfation in intact cells. *Biochem Biophys Res Commun* **141**, 870-877 (1986).
86. F. Safaiyan *et al.*, Selective effects of sodium chlorate treatment on the sulfation of heparan sulfate. *J Biol Chem* **274**, 36267-36273 (1999).
87. A. Basu *et al.*, Quantitative HILIC-Q-TOF-MS Analysis of Glycosaminoglycans and Non-reducing End Carbohydrate Biomarkers via Glycan Reductive Isotopic Labeling. *Anal Chem* **97**, 17490-17500 (2025).
88. V. Singh, R. Bhat, Proteoglycan desulfation: a critical step in oncogenesis? *Front Biosci (Landmark Ed)* **25**, 760-780 (2020).
89. S. Superina, A. Borovina, B. Ciruna, Analysis of maternal-zygotic ugdh mutants reveals divergent roles for HSPGs in vertebrate embryogenesis and provides new insight into the initiation of left-right asymmetry. *Dev Biol* **387**, 154-166 (2014).
90. K. Itoh, S. Y. Sokol, Heparan sulfate proteoglycans are required for mesoderm formation in Xenopus embryos. *Development* **120**, 2703-2711 (1994).
91. G. W. Yip, P. Ferretti, A. J. Copp, Heparan sulphate proteoglycans and spinal neurulation in the mouse embryo. *Development* **129**, 2109-2119 (2002).
92. M. Gupta *et al.*, Fine-tuning of Fgf8 morphogen gradient by heparan sulfate proteoglycans in the extracellular matrix. *Biophys J* **124**, 996-1010 (2025).
93. M. Fürthauer, J. Van Celst, C. Thisse, B. Thisse, Fgf signalling controls the dorsoventral patterning of the zebrafish embryo. *Development* **131**, 2853-2864 (2004).
94. G. Diez-Roux, A. Ballabio, Sulfatases and human disease. *Annu Rev Genomics Hum Genet* **6**, 355-379 (2005).
95. C. Settembre *et al.*, Systemic inflammation and neurodegeneration in a mouse model of multiple sulfatase deficiency. *Proc Natl Acad Sci U S A* **104**, 4506-4511 (2007).
96. S. L. Gande *et al.*, Paralog of the formylglycine-generating enzyme--retention in the endoplasmic reticulum by canonical and noncanonical signals. *Febs j* **275**, 1118-1130 (2008).
97. F. Milz *et al.*, Cooperation of binding sites at the hydrophilic domain of cell-surface sulfatase Sulf1 allows for dynamic interaction of the enzyme with its substrate heparan sulfate. *Biochim Biophys Acta* **1830**, 5287-5298 (2013).

98. C. Marques, C. A. Reis, R. R. Vivès, A. Magalhães, Heparan Sulfate Biosynthesis and Sulfation Profiles as Modulators of Cancer Signalling and Progression. *Front Oncol* **11**, 778752 (2021).
99. B. Ohkawara, T. S. Yamamoto, M. Tada, N. Ueno, Role of glypican 4 in the regulation of convergent extension movements during gastrulation in Xenopus laevis. *Development* **130**, 2129-2138 (2003).
100. R. Muñoz, M. Moreno, C. Oliva, C. Orbenes, J. Larraín, Syndecan-4 regulates non-canonical Wnt signalling and is essential for convergent and extension movements in Xenopus embryos. *Nat Cell Biol* **8**, 492-500 (2006).
101. J. Topczewski *et al.*, The zebrafish glypican knypek controls cell polarity during gastrulation movements of convergent extension. *Dev Cell* **1**, 251-264 (2001).
102. B. De Cat *et al.*, Processing by proprotein convertases is required for glypican-3 modulation of cell survival, Wnt signaling, and gastrulation movements. *J Cell Biol* **163**, 625-635 (2003).
103. M. C. Brickman, J. C. Gerhart, Heparitinase inhibition of mesoderm induction and gastrulation in Xenopus laevis embryos. *Dev Biol* **164**, 484-501 (1994).
104. E. Moro *et al.*, A novel functional role of iduronate-2-sulfatase in zebrafish early development. *Matrix Biol* **29**, 43-50 (2010).
105. J. R. Meyers *et al.*, Sulf1 modulates BMP signaling and is required for somite morphogenesis and development of the horizontal myoseptum. *Dev Biol* **378**, 107-121 (2013).
106. J. F. Colas, J. M. Launay, J. L. Vonesch, P. Hickel, L. Maroteaux, Serotonin synchronises convergent extension of ectoderm with morphogenetic gastrulation movements in Drosophila. *Mech Dev* **87**, 77-91 (1999).
107. B. Schaerlinger, J. M. Launay, J. L. Vonesch, L. Maroteaux, Gain of affinity point mutation in the serotonin receptor gene 5-HT2Dro accelerates germband extension movements during Drosophila gastrulation. *Dev Dyn* **236**, 991-999 (2007).
108. S. Karki *et al.*, Serotonin signaling regulates actomyosin contractility during morphogenesis in evolutionarily divergent lineages. *Nat Commun* **14**, 5547 (2023).
109. G. H. Baeg, X. Lin, N. Khare, S. Baumgartner, N. Perrimon, Heparan sulfate proteoglycans are critical for the organization of the extracellular distribution of Wingless. *Development* **128**, 87-94 (2001).
110. S. Veerapathiran *et al.*, Wnt3 distribution in the zebrafish brain is determined by expression, diffusion and multiple molecular interactions. *Elife* **9**, (2020).
111. B. Ohkawara, A. Glinka, C. Niehrs, Rspo3 binds syndecan 4 and induces Wnt/PCP signaling via clathrin-mediated endocytosis to promote morphogenesis. *Dev Cell* **20**, 303-314 (2011).
112. J. D. Axelrod, J. R. Miller, J. M. Shulman, R. T. Moon, N. Perrimon, Differential recruitment of Dishevelled provides signaling specificity in the planar cell polarity and Wingless signaling pathways. *Genes Dev* **12**, 2610-2622 (1998).
113. T. J. Park, R. S. Gray, A. Sato, R. Habas, J. B. Wallingford, Subcellular localization and signaling properties of dishevelled in developing vertebrate embryos. *Curr Biol* **15**, 1039-1044 (2005).
114. S. Sarrazin, W. C. Lamanna, J. D. Esko, Heparan sulfate proteoglycans. *Cold Spring Harb Perspect Biol* **3**, (2011).
115. K. Hayashida, R. S. Aquino, P. W. Park, Coreceptor functions of cell surface heparan sulfate proteoglycans. *Am J Physiol Cell Physiol* **322**, C896-c912 (2022).
116. Y. Mii *et al.*, Roles of two types of heparan sulfate clusters in Wnt distribution and signaling in Xenopus. *Nat Commun* **8**, 1973 (2017).
117. Q. Tao *et al.*, Maternal wnt11 activates the canonical wnt signaling pathway required for axis formation in Xenopus embryos. *Cell* **120**, 857-871 (2005).
118. Y. G. Brickman *et al.*, Structural modification of fibroblast growth factor-binding heparan sulfate at a determinative stage of neural development. *J Biol Chem* **273**, 4350-4359 (1998).
119. V. Nurcombe, M. D. Ford, J. A. Wildschut, P. F. Bartlett, Developmental regulation of neural response to FGF-1 and FGF-2 by heparan sulfate proteoglycan. *Science* **260**, 103-106 (1993).
120. M. Westerfield, *The zebrafish book. A guide for the laboratory use of zebrafish (Danio rerio).* . (Univ. of Oregon Press Eugene, Oregon, USA, 2000), vol. 4th edition.
121. C. B. Kimmel, W. W. Ballard, S. R. Kimmel, B. Ullmann, T. F. Schilling, Stages of embryonic development of the zebrafish. *Developmental Dynamics* **203**, 253-310 (1995).
122. J. Zhang, W. S. Talbot, A. F. Schier, Positional cloning identifies zebrafish one-eyed pinhead as a permissive EGF-related ligand required during gastrulation. *Cell* **92**, 241-251 (1998).
123. M. A. Moreno-Mateos *et al.*, CRISPRscan: designing highly efficient sgRNAs for CRISPR-Cas9 targeting in vivo. *Nat Methods* **12**, 982-988 (2015).

124. A. Burger *et al.*, Maximizing mutagenesis with solubilized CRISPR-Cas9 ribonucleoprotein complexes. *Development* **143**, 2025-2037 (2016).
125. D. Y. Guschin *et al.*, A rapid and general assay for monitoring endogenous gene modification. *Methods Mol Biol* **649**, 247-256 (2010).
126. K. Sampath *et al.*, Induction of the zebrafish ventral brain and floorplate requires cyclops/nodal signalling. *Nature* **395**, 185-189 (1998).
127. D. G. Gibson *et al.*, Enzymatic assembly of DNA molecules up to several hundred kilobases. *Nat Methods* **6**, 343-345 (2009).
128. C. Thisse, B. Thisse, High-resolution in situ hybridization to whole-mount zebrafish embryos. *Nature Protocols* **3**, 59-69 (2008).
129. A. Alaniz Emig, M. L. K. Williams, Generation of Naïve Blastoderm Explants from Zebrafish Embryos. *J Vis Exp*, (2021).
130. D. Ershov *et al.*, TrackMate 7: integrating state-of-the-art segmentation algorithms into tracking pipelines. *Nat Methods* **19**, 829-832 (2022).